# Moist Surface Frontogenesis Associated with Interior Potential Vorticity Anomalies in a Semigeostrophic Model

MICHAEL T. MONTGOMERY AND BRIAN F. FARRELL

*Department of Earth and Planetary Sciences, Harvard University, Cambridge, Massachusetts*

(Manuscript received 22 March 1990, in final form 9 August 1990)

ABSTRACT

We previously examined surface frontogenesis as an initial value problem in a dry inviscid semigeostrophic Eady model focusing on the frontal dynamics associated with interior potential vorticity anomalies. This work explores frontogenesis associated with potential vorticity anomalies in the presence of latent heat release using a generalization of the two-dimensional semigeostrophic Eady model that insures that the heating term gives correct asymptotic behavior at high and low temperatures. A variety of initial conditions are considered in which upper-level potential vorticity disturbances induce strong positive potential vorticity anomalies near the lower surface. With uniform interior potential vorticity, baroclinic coupling between the upper and surface induced disturbance is weak despite a near neutral moist stability. On the other hand, examples of initial disturbances with interior potential vorticity show greatly enhanced baroclinic coupling between upper and lower disturbances. Comparison with a recent observational study suggests these represent a simple phenomenological description of squall line development.

We also find that latent heat release destabilized surface concentrated disturbances which do not intensify in the dry problem. These frontal developments are not primarily baroclinic. Rather, the source of energy is latent heat released in ascent regions and the attendant generation of surface potential vorticity. Development is slow in comparison to baroclinic frontogenesis but is not dependent on the presence of large amplitude perturbations. This diabatic surface development also appears in examples involving upper-level potential vorticity disturbances as a slow intensification of meridional surface winds following the more rapid baroclinic interaction between upper- and lower-level disturbances. Examples suggestive of observed polar low development comprise an initial baroclinic growth phase followed by a slow intensification due to diabatic effects.

## 1. Introduction

Previously, we examined dry surface frontogenesis as an initial value problem in an inviscid two-dimensional semigeostrophic Eady model concentrating on frontal dynamics associated with interior potential vorticity anomalies (Montgomery and Farrell 1990). We found rapid surface frontogenesis for properly configured disturbances in the absence of exponential modal growth. In this work we extend the previous results to include new surface frontogenetic processes associated with potential vorticity anomalies in the presence of latent heat release.

A variety of parameterizations have been applied to represent hydrological processes within atmospheric cyclones and fronts including conditional instability of the second kind (CISK) for the growth of hurricane depressions (Charney and Eliassen 1964); Wave-CISK for quasi-geostrophic baroclinic instability (Stevens and Lindzen 1978; Mak 1982; Snyder and Lindzen 1989) and the approach of Emanuel, Fantini and Thorpe (1989) (EFT) for surface frontogenesis. The idea behind CISK involves cooperative interaction between cumulus clouds and large-scale moisture convergence. CISK assumes an atmosphere conditionally unstable to upright moist convection. An approach similar to EFT is adopted as an alternative to CISK. This approach assumes ascending parcels conserve saturated entropy. All water rains out during the parcel's ascent and on descent the parcel conserves dry entropy. In contrast with CISK models this approach assumes an environment conditionally stable to upright parcel displacements but nearly neutral along absolute momentum surfaces.

The dynamics of growing normal modes with initially uniform interior potential vorticity was examined by EFT. For these disturbances the effect of latent heat release in the limit of moist neutrality was shown to approximately double the growth rate of the most unstable dry normal mode, and to slightly modify the surface frontal structure arising from exponentially growing dry normal modes. Thus, for disturbances of unstable normal mode form, latent heat release serves only to modify dry frontogenesis.

Simple arguments imply that latent heat release enhances development of baroclinic systems. A widely

*Corresponding author address:* Dr. Michael T. Montgomery, Dept. of Earth and Planetary Sciences, Harvard University, Pierce Hall, 29 Oxford Street, Cambridge, MA 02138.

accepted procedure for parameterizing the influence of diabatic processes on growing baroclinic waves is to reduce the dry static stability. If the results of EFT are used as a guide, reducing the static stability by a factor of two in the Eady model causes the wavelength of most rapid exponential growth to decrease from 3900 km to 2800 km, its associated nondimensional growth rate increases from .31 to .43, and the short-wave cutoff decreases from 2500 km to 1800 km. Thus, reducing the static stability enhances development and widens the range of unstable wavenumbers.

Condensation within a disturbance may produce unique frontogenetic processes on the synoptic and mesoscale which have no counterpart in a dry atmosphere. Consider an upper-level potential vorticity perturbation embedded in a baroclinic jet. If in ascent regions we assume air to be saturated, positive potential vorticity will be induced below and downstream of the upper anomaly and subsequent baroclinic interaction between these structures may result in rapid surface frontogenesis. This kind of surface frontogenesis will not occur in a dry Eady model which has no sources of potential vorticity. In cases of near moist neutrality throughout the depth of the troposphere the upper/lower vorticity couplet can produce rapid surface frontogenesis. With increased moist stability the upper disturbance passes over the surface system with negligible surface development.

In recent work (Montgomery and Farrell 1990) the importance of transient processes in the dry two-dimensional Eady model with nonuniform potential vorticity was demonstrated for stable short wavelength disturbances. Here, we find that condensation within a short-wave disturbance induces transient frontogenetic processes which have no dry counterpart. While interior potential vorticity perturbations have long been associated with cyclogenesis (Eliassen and Kleinschmidt 1957) this role is becoming more widely appreciated (Farrell 1982, 1984, 1985; Hoskins et al. 1985; Whitaker et al. 1988; Davis 1990).

In section 2 the model equations are developed; in section 3 a variety of time integrations are presented, to highlight the physical processes. We conclude by summarizing our results and point to future work.

## 2. Model formulation

A useful idealization is to represent the process of condensation in extratropical cyclones and fronts by assuming ascending parcels to be saturated throughout their bulk ascent with all water precipitating out during ascent: a pseudoadiabatic ascent approximately conserving saturated entropy. Descending air parcels are assumed to be free of water and to conserve dry entropy. Evaporation of liquid water is neglected. While observations do not contradict this idealization it is a simplification of complex hydrology. In moist regions the atmosphere is assumed statically stable, but nearly neutral to upright saturated displacements and it is assumed that moist convection maintains this state of near neutrality. A generalization that permits positive moist stability at high levels and qualitative temperature dependence in the latent heating is developed below.

The flows considered are inviscid and possess long time scales compared to gravity and acoustic periods. This motivates the use of a balance approximation which filters these higher frequency modes. The dry two-dimensional semigeostrophic Boussinesq Eady Model of Hoskins and Bretherton (1972) captures the rapidity of the frontogenesis process by retaining advection of the ageostrophic winds producing strong convergence and infinite relative vorticity in finite time. Early research with this system predicted frontal structures qualitatively resembling observational data (Williams 1967; Blumen 1980). The success of the dry model suggests using a similar balanced framework for moist frontal dynamics. A more complete discussion of this balanced model can be found in EFT.

In terms of the modified geopotential $\Phi = \phi + v_g^2/2$, the semigeostrophic Eady model takes a simple form when it is formulated in geostrophic coordinates and the computational advantages of modeling fronts in these coordinates are well known (Hoskins 1975). Here, integrations are carried out in the geostrophic coordinates given by:

$$X = x + v_g/f$$

$$Y = y - u_g/f$$

$$Z = z$$

$$T = t \tag{2.1}$$

and all fields are transformed back to real coordinates via (2.1).

In geostrophic coordinates the moist equivalent potential vorticity $Q_{ge}$ plays the role of the moist vertical stability in the equation for saturated entropy conservation. The current approach consists in rephrasing the vertical stability assumption in terms of $Q_{ge}$ in geostrophic coordinates. This corresponds to assuming that the initial $Q_{ge}$ distribution is everywhere small and positive and is equivalent to assuming near moist neutrality along absolute momentum surfaces given by $M \equiv fx + v_g = \text{const}$. Thus, the model given by (2.4, 2.5) is formally identical to the model described by EFT, though our interpretation of the moisture parameterization is somewhat different.

The two-dimensional Eady model consists of a two-dimensional wave field superimposed upon a hydrostatic basic state with a zonally homogeneous constant shear in thermal wind balance with a constant meridional temperature gradient. The basic state is:

$$\bar{U}_g = SZ$$
$$\bar{V}_g = 0, \quad \bar{U}_{ag} = 0, \quad \bar{V}_{ag} = 0, \quad \bar{W} = 0$$
$$\bar{\Phi}(Y, Z) = -fSYZ + (N_0^2 Z^2/2) + gZ$$
$$\bar{\Theta}(Y, Z) = -g^{-1}\theta_0 fSY + g^{-1}N_0^2\theta_0 Z + \theta_0, \quad (2.2)$$

representing an exact solution of the inviscid momentum and moist adiabatic equations given in EFT.

The basic state is disturbed with the amplitude of the disturbances not being assumed small. In accord with the two-dimensionality constraint on the disturbance field, X-periodic solutions are sought in the form:

$$U_{\text{total}} = \bar{U}_g + u_{ag}(X, Z, T)$$
$$V_{\text{total}} = v_g(X, Z, T)$$
$$W_{\text{total}} = w(X, Z, T)$$
$$\Theta_{\text{total}} = \bar{\Theta}(Y, Z) + \theta(X, Z, T)$$
$$\Phi_{\text{total}} = \bar{\Phi}(Y, Z) + \Phi(X, Z, T). \quad (2.3)$$

Dry and moist equivalent potential vorticity are designated as $Q_g$ and $Q_{ge}$, respectively. All remaining fields are deduced from the equation relating $Q_g$ to $\Phi$ and the Sawyer–Eliassen circulation equation for the cross frontal streamfunction $\Psi$. The equations of motion are:

$$\left(\frac{\partial}{\partial T} + SZ\frac{\partial}{\partial X}\right)Q_g + w\frac{\partial}{\partial Z}Q_g = J\frac{\partial}{\partial Z}\left[w^*\left(Q_g - \frac{\Gamma_m}{\Gamma_d}Q_{ge}\right)\right] \quad (2.4a)$$

$$\left(\frac{\partial}{\partial T} + SZ\frac{\partial}{\partial X}\right)Q_{ge} + w\frac{\partial}{\partial Z}Q_{ge} = 0 \quad (2.4b)$$

$$\left(\frac{\partial}{\partial T} + SZ\frac{\partial}{\partial X}\right)\theta = \frac{f\theta_0}{g}Sv_g, \quad \text{on} \quad Z = 0, H \quad (2.4c)$$

$$Q_g = \left(\frac{\partial^2\Phi}{\partial Z^2} + N_0^2\right)\left(1 - \frac{1}{f^2}\frac{\partial^2\Phi}{\partial X^2}\right)^{-1} \quad (2.4d)$$

$$\frac{\partial}{\partial X}\left(Q_{g_{\text{eff}}}\frac{\partial\psi}{\partial X}\right) + f^2\frac{\partial^2\psi}{\partial Z^2} = -2fS\frac{\partial v_g}{\partial X} \quad (2.4e)$$

where

1) Updrafts are saturated and downdrafts are free of water.

2) The right-hand side of (2.4a) is set to zero in downdrafts (i.e., when $w < 0$) and the quantity $\Gamma_m/\Gamma_d$ represents the ratio of moist adiabatic to dry adiabatic lapse rates.

3) The quantity

$$Q_{g_{\text{eff}}} = \begin{cases} \Gamma_m Q_{ge}/\Gamma_d & \text{if} \quad w > 0 \\ Q_g & \text{if} \quad w < 0. \end{cases} \quad (2.4f)$$

4) The starred ageostrophic velocities and the unstarred ageostrophic velocities are obtained via the expressions:

$$u^*_{ag} = +\partial\psi/\partial Z \quad (2.5a)$$
$$w^* = -\partial\psi/\partial X \quad (2.5b)$$
$$w = Jw^* \quad (2.5c)$$
$$u_{ag} = u^*_{ag} - \frac{w}{f^2}\frac{\partial^2\Phi}{\partial Z\,\partial X} \quad (2.5d)$$
$$J = [1 - f^{-2}(\partial^2\Phi/\partial X^2)]^{-1} \quad (2.5e)$$

5) The fields in physical coordinates $(x, z)$ are obtained from the geostrophic coordinates via:

$$x = X - f^{-1}v_g(X, Z, T)$$
$$z = Z. \quad (2.5f)$$

The $J$ in Eq. (2.5e) denotes the Jacobian of the transformation between the real $(x, z)$ and geostrophic $(X, Z)$ coordinates. It also equals the ratio of the vertical component of absolute vorticity to $f$: $J = 1 + f^{-1}\zeta = 1 + f^{-1}\partial v_g/\partial x$. Regions in geostrophic space where $J$ is greater than unity correspond to $x$-contracted regions in real space, whereas regions where it is less than unity correspond to $x$-elongated regions in real space.

The special case of a two-layer approximation to the system (2.4)–(2.5), which neglects the temporal change in $Q_g$ in the middle level, has been discussed by EFT. By its nature however a two-layer approximation is unable to resolve dynamics dominated by interaction of potential vorticity anomalies with substantial vertical structure. The method of solution adopted in this paper is computational, with up to 65 levels in the vertical to insure convergence. An outline of the solution method follows.

Integration of the system (2.4) is performed in a zonally periodic rectangular domain of nondimensional length $L$ bounded in the vertical by two rigid lids representative of the earth's surface and tropopause. A sketch of the computational domain is given in Fig. 1. Boundary conditions require periodicity in $X$, up dated values of $\theta = (\theta_0/g)(\partial\Phi/\partial Z)$ along $Z = 0, H$ to invert (2.4d) for $\Phi$, and a vanishing cross-frontal

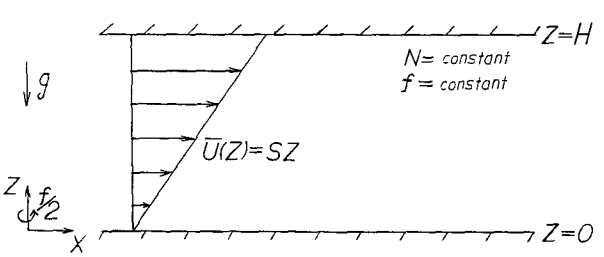


FIG. 1. Sketch of the two-dimensional Eady model geometry defined in section 2.

streamfunction along $Z = 0, H$ to invert (2.4e) for $\psi$. For simplicity the initial disturbances in $\Phi$ are sinusoidal in $X$ with a single wavenumber $k$. The horizontal resolution is therefore $\delta x = (2\pi/Nk)1000$ in kilometers, where $N$ is either 65 or 33. The integration procedure is the same as in Montgomery and Farrell (1990) except that both elliptic Eqs. (2.6c, 2.6d) are solved via simultaneous over-relaxation (SOR) with a relaxation parameter of 1.8 (Press et al. 1986).

The initial condition for the integration requires specification of the geopotential $\Phi$ throughout the entire domain including its values on the rigid lids. The dry potential vorticity can then be computed via (2.4d). Determination of the initial moist potential vorticity is discussed below. Ageostrophic wind fields consistent with the initial geopotential are obtained by inverting (2.4e) for $\psi$ using (2.5). Integration proceeds by advancing both the dry and moist potential vorticity and adiabatic equations [(2.4a), (2.4b) and (2.4c), respectively] in time, and then solving the diagnostic equations for the updated geopotential $\Phi$ and cross-frontal streamfunction $\psi$. The process is repeated for each time step.

In EFT the equivalent moist potential vorticity $Q_{ge}$ was taken to be small, positive, and uniform throughout the flow domain making explicit integration of Eq. (2.4b) unnecessary. They investigated the effect of latent heat release on exponentially growing normal modes of the dry Eady problem whose dry potential vorticity $Q_g$ was initially uniform. In general, however, one cannot independently specify $Q_{ge}$ and $Q_g$ since the two quantities are related thermodynamically. From their definition in geostrophic space:

$$Q_g = gJ(\partial \ln\theta/\partial Z) \tag{2.6a}$$

$$Q_{ge} = gJ(\partial \ln\theta_e/\partial Z) \tag{2.6b}$$

where

$$\theta = T(p_s/p)^{R/c_p} = \text{potential temperature} \tag{2.6c}$$

$$\theta_e \approx \theta \exp(ml_v/c_pT)$$

$$= \text{equivalent potential temperature} \tag{2.6d}$$

and $T$ = thermodynamic temperature, $p_s$ = reference surface pressure (1000 mb), $R$ is the ideal gas constant, $c_p$ is the specific heat at constant pressure, $m$ = mixing ratio, and $l_v$ = latent heat of condensation per unit mass.

Consider the qualitative dependence of $Q_{ge}$ on temperature and recall the exponential temperature dependence of the saturation vapor pressure $e_s$ along the vapor–liquid saturation curve. At low temperatures, say 260 K, $e_s$ is approximately 3 mb which is much smaller than its value at 300 K of 35 mb. Since the latent heating is proportional to the mixing ratio $m \approx 0.622e_s/p_d$, where $p_d$ is dry air pressure, the magnitude of latent heating should be much smaller at low temperatures than at high temperatures. Consequently, the potential vorticity induction term on the right-hand side of (2.4a) will be maximum at high temperatures and diminish with decreasing temperature. As the mixing ratio approaches zero $\Gamma_m/\Gamma_d \to 1$, $\theta_e \to \theta$ and $Q_{ge} \to Q_g$. Hence, for a nonisothermal atmosphere in which the temperature decreases with height, the induction term should be smaller aloft than at the surface for similar vertical velocity magnitudes. Conversely, for an approximately isothermal atmosphere having a vertically extended near moist neutral region, the magnitude of the induction term should be large throughout the atmospheric column.

We wish to explore a variety of moist frontal processes with:

1) A moisture parameterization that exhibits the asymptotic temperature dependence outlined above,

2) the flexibility of integrating flows with initially nonuniform potential vorticity.

It is clear that $Q_{ge}$ can no longer be taken as a small uniform constant and an alternative parameterization follows.

The ratio between (2.6a) and (2.6b) results in

$$\frac{Q_{ge}}{Q_g} = \left(\frac{\partial \ln\theta_e}{\partial Z}\right)\left(\frac{\partial \ln\theta}{\partial Z}\right)^{-1} \equiv S_e. \tag{2.7a}$$

In regions of near moist neutrality we assume that the equivalent moist potential vorticity is small and positive. It is also assumed that in ascent regions moist convection maintains the lapse rate in the numerator of the $S_e$ definition (2.7a) to be always nearly moist adi abatic. However, since convective motions have been filtered in this model it is impossible to directly evaluate this lapse rate, and hence impossible to determine $S_e$, in terms of the computed fields. Regardless of how $S_e$ is determined is must be compatible with the thermodynamic constaints above. A phenomenological prescription for a nonisothermal atmosphere that meets these requirements is obtained for $S_e$ functions varying monotonically in the vertical, starting small and positive near the earth's surface and increasing with height. This choice is consistent with conservation of $Q_{ge}$ in ascending regions provided:

$$\frac{D_gS_e}{DT} = -\frac{S_e}{Q_g}\frac{D_gQ_g}{DT}. \tag{2.8a}$$

Now, since regions of descending air are assumed free of water we set $Q_{ge} = Q_g$ in these regions and replace the right-hand side of (2.8a) by zero. Equation (2.8a) replaces Eq. (2.4b) and in (2.8a) the full advection operator in geostrophic coordinates is abbreviated as

$$\frac{D_g}{DT} \equiv \frac{\partial}{\partial T} + SZ\frac{\partial}{\partial X} + w\frac{\partial}{\partial Z}. \tag{2.8b}$$

The dry potential vorticity equation becomes

$$\left(\frac{\partial}{\partial T} + SZ\frac{\partial}{\partial X}\right)Q_g + w\frac{\partial}{\partial Z}Q_g = J\frac{\partial}{\partial Z}\left[w^*Q_g\left(1 - \frac{\Gamma_m}{\Gamma_d}S_e\right)\right]. \quad (2.9)$$

If we further assume that $\Gamma_m S_e(X, Z; T)/\Gamma_d \approx \Gamma_m S_e(Z)/\Gamma_d \equiv R(Z)$, the temporal and spatial change in $S_e$ due to advection can be neglected. This quasi-static approximation packages the moisture parameterization into a vertically varying function $R(Z)$, the validity of which has been confirmed for short to moderate time integrations. Results of the upcoming section are not qualitatively affected by this approximation and, unless otherwise stated, all results are computed by holding $S_e$ constant in time.

Two simple choices for the $R$ function are given by

$$R(Z) \equiv R_0 \quad (2.10a)$$

$$R(Z) = R_0 + (1 - R_0)Z. \quad (2.10b)$$

Definitions (2.10a) and (2.10b) correspond physically to a deep and surface confined near moist neutral region, respectively. If in (2.10a) we take $R_0 \to 0$ and assume $Q_g$ to remain bounded, we recover the moisture parameterization made in EFT which assumed uniform and small $Q_{ge}$. The solutions of EFT are confirmed with the present approach in the limit $R \to 0$. The condition of small moist stability generally corresponds to small $R_0$ and the present formulation includes a parameterization of vertical temperature dependence in the heating term.

The parameters in the system described by (2.4), (2.5), and (2.9) can be reduced by an appropriate choice of dimensionless variables. The choice of scaling is the same as in Montgomery and Farrell (1990) where the explicit dependence on the Rossby number $= U_0(f_0L_0)^{-1} = S(Q_{g0})^{-1/2} \equiv (\mathrm{Ri})^{-1/2}$ was eliminated. Representative values of the parameters for the two-dimensional Eady model and the relation between the dimensional fields and the nondimensional (hat) variables are listed in Table 1. This dimensionless system has a zonal scale of 1000 km, a vertical scale of 10 km, one advective time unit corresponds to 9.25 h, both the zonal and meridional velocity scale are 100 m s$^{-1}$, the potential temperature scale is 30 K, and the ageostrophic scaling for $u_{ag}$ and w are 30 m s$^{-1}$ and 30 cm s$^{-1}$, respectively. Hereafter hat notation will be dropped.

The anomalous part of the dry potential vorticity is best displayed explicitly by writting

$$Q_g = 1 + q_g.$$

In terms of the anomalous potential vorticity $q_g$, the dimensionless equations for the disturbance field become:

TABLE 1. Representative values of parameters for the two-dimensional Eady model and the relation between dimensional (tilde) fields and nondimensional hatted variables defined in section 2.

| | |
|---|---|
| $Q_{g0} = N_0^2$ | $= 10^{-4}$ s$^{-2}$ |
| $H$ | $= 10$ km |
| $f$ | $= 10^{-4}$ s$^{-1}$ |
| $S$ | $= 3$ m s$^{-1}$ km$^{-1}$ |
| $L_R = Q_{g0}^{1/2}Hf^{-1}$ | $= 1000$ km |
| $T = L_RU^{-1} = \sqrt{\mathrm{Ri}}f^{-1}$ | $= 9.25$ h |
| $\tilde{\Phi} = Q_{g0}H^2\hat{\Phi}$ | $= (10^4$ m$^2$ s$^{-2})\hat{\Phi}$ |
| $\tilde{Q}_g = N_0^2\hat{Q}_g$ | $= 10^{-4}$ s$^{-2}\hat{Q}_g$ |
| $\tilde{v}_g = HQ_{g0}^{1/2}\hat{v}_g$ | $= (100$ m s$^{-1})\hat{v}_g$ |
| $\tilde{\theta} = g^{-1}\theta_0Q_{g0}H\hat{\theta}$ | $= (30$ K$)\hat{\theta}$ |
| $\tilde{u}_{ag} = SH\hat{u}_{ag}$ | $= (30$ m s$^{-1})\hat{u}_{ag}$ |
| $\tilde{w} = Q_{g0}^{-1/2}fSH\hat{w}$ | $= (30$ cm s$^{-1})\hat{w}$ |

$$\left(\frac{\partial}{\partial T} + Z\frac{\partial}{\partial X}\right)q_g + w\frac{\partial}{\partial Z}q_g = J\frac{\partial}{\partial Z}\{w^*(1 + q_g)[1 - R(Z)]\} \quad (2.11a)$$

$$\left(\frac{\partial}{\partial T} + Z\frac{\partial}{\partial X}\right)\theta = \frac{\partial\Phi}{\partial X}, \quad \text{on} \quad Z = 0, 1 \quad (2.11b)$$

$$(q_g + 1)\frac{\partial^2\Phi}{\partial X^2} + \frac{\partial^2\Phi}{\partial Z^2} = q_g \quad (2.11c)$$

$$\frac{\partial}{\partial X}\left(Q_{g_{\mathrm{eff}}}\frac{\partial\psi}{\partial X}\right) + \frac{\partial^2\psi}{\partial Z^2} = -2\frac{\partial^2\Phi}{\partial X^2} \quad (2.11d)$$

where:

1) The right-hand side of (2.11a) is replaced by zero when $w < 0$.

2) The quantity

$$Q_{g_{\mathrm{eff}}} = \begin{cases}(1 + q_g)R(Z) & \text{when} \quad w > 0\\ (1 + q_g) & \text{when} \quad w < 0\end{cases} \quad (2.11e)$$

3) $R(Z)$ is given by (2.10).

4) The starred ageostrophic velocities and the unstarred ageostrophic velocities are obtained via the expressions:

$$u_{ag}^* = +\partial\psi/\partial Z \quad (2.12a)$$

$$w^* = -\partial\psi/\partial X \quad (2.12b)$$

$$w = Jw^* \quad (2.12c)$$

$$u_{ag} = u_{ag}^* - w(\partial^2\Phi/\partial Z\,\partial X) \quad (2.12d)$$

$$J = [1 - (\partial^2\Phi/\partial X^2)]^{-1}. \quad (2.12e)$$

5) The fields in physical coordinates $(x, z)$ are obtained via the transformation from geostrophic coordinates:

$$x = X - v_g(X, Z, T)$$
$$z = Z. \qquad (2.12f)$$

6) The boundary conditions on the geopotential $\Phi$ are that it remain periodic in $X$ and satisfy $\theta = \partial\Phi/\partial Z$ along the horizontal boundaries $Z = 0, 1$. The boundary conditions on the streamfunction $\psi$ are that it remain periodic in $X$ and vanish on the horizontal boundaries $Z = 0, 1$.

The system (2.11) contains distinct features not present in the dry model obtained by setting $R(Z) \equiv 1$ that was investigated previously (Montgomery and Farrell 1990). The first is the local creation and destruction of potential vorticity $Q_g$ in ascent regions due to the nonzero right-hand side of Eq. (2.11a). With no diabatic forcing on the horizontal boundaries $Z = 0, 1$, it is easily shown that latent heat release does not change the net mass-integrated potential vorticity of the flow (Thorpe and Emanuel 1985). Despite this global constraint, local induction of potential vorticity anomalies in the vicinity of preexisting anomalies associated with old cyclones, surface fronts, or tongues of stratospheric air, may have a dramatic impact on the frontal dynamics through interactions between these potential vorticity structures. A second feature is the effective static stability in the cross-frontal streamfunction Eq. (2.11d): the effective potential vorticity $Q_{g_{\text{eff}}}$ plays the same role as the static stability in the $\psi$ equation. Therefore, as $R_0 \to 0$, ascent regions will tend to extend vertically much more readily than descent regions. Finally, the effective static stability for the geopotential Eq. (2.11c) is $Q_g = 1 + q_g$ and hence is much larger than the effective static stability of the cross-frontal equation as $R_0 \to 0$.

With respect to updraft regions the model (2.11, 2.12) may be interpreted as operating along the vapor–liquid saturation curve. Complications associated with evaporation, entrainment, and microphysics, such as nucleation etc., have been neglected and no distinction is made between latent heat of condensation and the latent heat of sublimation. Despite these simplifications this phenomenological model of an inviscid moist atmosphere is sufficient to capture essential physics of latent heat release for large-scale baroclinic midlatitude frontal flows. For cases involving a near moist neutral isothermal atmosphere the formula (2.10a) for $R$ should be used. Alternatively, (2.10b) should be used for a nonisothermal atmosphere whose near neutral stability region is confined to lower levels.

## 3. Moist frontogenesis studies

Moist surface frontogenesis for the system (2.11, 2.12) was investigated by EFT in the limit of near moist neutrality ($Q_{ge} \to 0$). They considered disturbances that were initially dry with uniform $Q_{ge}$, and $Q_g$, and concentrated on unstable normal modes with wavenumbers close to or smaller than the short-wave cutoff of the dry Eady problem. We extend these results by considering the moist dynamics of interior potential vorticity anomalies, focusing on the physical interactions between these potential vorticity structures rather than on the behavior of the corresponding normal modes. In particular, we focus on potential vorticity disturbances with wavenumbers greater than the short-wave cutoff of the dry two-dimensional Eady problem, and therefore absent of exponential growth in the dry problem.

The importance of short-wave potential vorticity disturbances in frontogenetic processes is suggested by the following considerations. Previous work on the dry counterpart of (2.11, 2.12) demonstrated rapid surface frontogenesis for finite amplitude interior potential vorticity anomalies possessing wavenumbers greater than the short-wave cut off (Montgomery and Farrell 1990). Also, in results reported by EFT, a positive surface induced potential vorticity anomaly of large amplitude and small zonal scale compared to the zonal scale of the initial disturbance is generated by latent heat release. Vertical advection which is included in semigeostrophic dynamics will lift these anomalies aloft. The anomaly is then free to interact with preexisting surface or interior potential vorticity features away from the frontal zone. Considerations such as these motivate further investigation of the dynamics of interior potential vorticity anomalies.

### *a. Induced self-development arising from upper-level forcing*

In the first series of examples, we investigate moist dynamics associated with the induction of low-level potential vorticity by preexisting upper-tropospheric short wavelength potential vorticity perturbations. Consider a positive upper-level potential vorticity disturbance embedded in a baroclinic jet. In order for this flow to remain in thermal wind balance, an ascending vertical motion field will arise below and downstream of the upper-level potential vorticity disturbance. If the air within the ascent region is saturated, latent heat release will induce a negative potential vorticity anomaly aloft and a positive potential vorticity anomaly near the earth's surface downstream of the upper-level perturbation. The induced surface anomaly may then interact baroclinically with the initial potential vorticity disturbance so that together the potential vorticity couplet taps the available potential energy of the mean flow leading to production of an intense surface cyclone or front. We wish to determine the circumstances under which surface development results from such a process.

Kleinschmidt (1950; Eliassen and Kleinschmidt 1957) believed that surface cyclones originated in this fashion. In this work this process will be referred to as

"induced self-development" (ISD for short). For surface development to occur from such a process it is necessary that a sizable vertical extent of the atmosphere be saturated. Also, simple considerations suggest another condition for the interaction of upper and surface induced potential vorticity anomalies: the Rossby penetration depth $R_d = f/Nk$, ($k$ being zonal wavenumber of either anomaly and $N$ the dry Brunt–Vaisala frequency), must be great enough to permit sufficient overlap between the surface and upper-level wind fields. Furthermore, if the winds aloft are so strong as to advect the upper anomaly over the lower anomaly before substantial interaction can take place, ISD will not be possible. Finally, frictional dissipation at the earth's surface implies the need for a sufficiently intense potential vorticity seed field at the surface to overcome energy loss in the boundary layer.

The first example adopts the moisture representation (2.10a) with $R = 0.01$ throughout the atmosphere. This value of $R$ is taken as representative of near moist neutral regions of large vertical extent (Joly and Thorpe 1989). The initial condition is an upper Eady dry normal mode with zonal wavenumber of $k = 2.5$:

$$\Phi(X, Z, 0) = \mathrm{Re}\{[A\cosh(kz) + B\sinh(kz)]\exp(ikx)\} \quad (3.1a)$$

where $c_r = 0.5676$, $A/B = -kc_r$, and $Bk = 1/27$ resulting in a nondimensional tropospheric maximum in $v_g$ and $\theta$ of .09 and .09, respectively. Dimensional values implied by this choice of parameters are meridional wind and potential temperature disturbance maxima of approximately 9 m s$^{-1}$ and 3 K at the model tropopause.

In the discussions that follow it is useful to recall that, from a mathematical point of view, one can append the $\theta$ perturbation to the potential vorticity $q_g$ and replace the boundary condition $\theta = \partial\Phi/\partial Z$ along horizontal surfaces with $\theta = 0$ (Bretherton 1966; Hoskins et al. 1985). Rather than viewing the $q_g$ and $\theta$ fields as separate, we may instead combine both fields into one generalized potential vorticity anomaly $q_{\mathrm{gen}}$ which has two primary contributions. The first consists of the interior potential vorticity anomaly $q_g$ and the second of two boundary terms each of which is proportional to a delta function multiplied by $\theta$ evaluated along the appropriate boundary. Positive values of $\theta$ are associated with positive delta functions in $q_{\mathrm{gen}}$ at the lower boundary while the converse holds for the upper boundary. For instance, with the initial condition (3.1a) the interior potential vorticity $q_g$ is identically zero but the generalized potential vorticity anomaly is mainly confined to the upper boundary $Z = 1$ in the form of a $\theta$ perturbation with a weak signature at the surface. The salient features of the solution for this example are shown in Figs. (2a,b) and important physical aspects are discussed in the following text.

#### 1) MERIDIONAL GEOSTROPHIC WIND

The vertical structure of the $v_g$ field is initially barotropic with maximum values at the model tropopause but there is also a slight surface signature of the upper mode having a maxima of 2 m s$^{-1}$ at $Z = 0$. At $T = 1$, evidence of baroclinic conversion of available potential energy to kinetic energy is seen through a westward tilt of the $v_g$ field with height against the background shear and an increase in northerly surface winds from 2 m s$^{-1}$ to approximately 7 m s$^{-1}$. The $v_g$ field at later times bears a close resemblance to a superposition of an upper and lower dry Eady mode that propagate eastward together as if phase locked, continuing to convert potential energy of the basic state into kinetic energy. At $T = 3$ a pronounced reduction in scale of the cyclonic vorticity region at the surface near $x = 1.9$ is evident. The phase locked structure travels eastward across the computational domain and reenters the western edge of the domain. Surface frontal collapse occurs at the western edge of the domain at approximately $T = 4.13$ corresponding to 38 hours. The maximum surface winds are 35 m s$^{-1}$ with a wind shear of nearly 65 m s$^{-1}$ across the frontal zone.

#### 2) JACOBIAN

The maximum in the Jacobian is initially 1.25 and occurs along the model tropopause with an associated relative vorticity of $0.25f$. At later times, however, the Jacobian maximum is found at the surface due to increased frontogenesis there compared to the tropopause. At the time of surface frontal collapse the Jacobian attains a value of 50 and corresponds to a relative vorticity of $49f$.

#### 3) POTENTIAL VORTICITY AND VERTICAL VELOCITY

The interior potential vorticity $q_g$ of this disturbance is initially zero. The potential vorticity anomaly is confined to the upper boundary $Z = 1$ in the form of a $\theta$ perturbation with a secondary anomaly in $\theta$ along the lower boundary. The smallness of $R_0$ combined with the constraint that the system remain in thermal wind balance requires strong updrafts below and downstream of the negative $\theta$ disturbance at the tropopause. This is seen in Fig. (2b). From Eq. (2.11a), the maximum rate of induction of interior potential vorticity $q_g$ in geostrophic coordinates occurs at the maximum of

$$J\frac{\partial[w^*(1 + q_g)(1 - R_0)]}{\partial Z}$$

For small amplitudes and early times one can ignore $q_g$ compared to unity, the distinction between $w$ and $w^*$, and the difference between real and geostrophic coordinates. Under these circumstances the maximum rate of induction of interior potential vorticity occurs

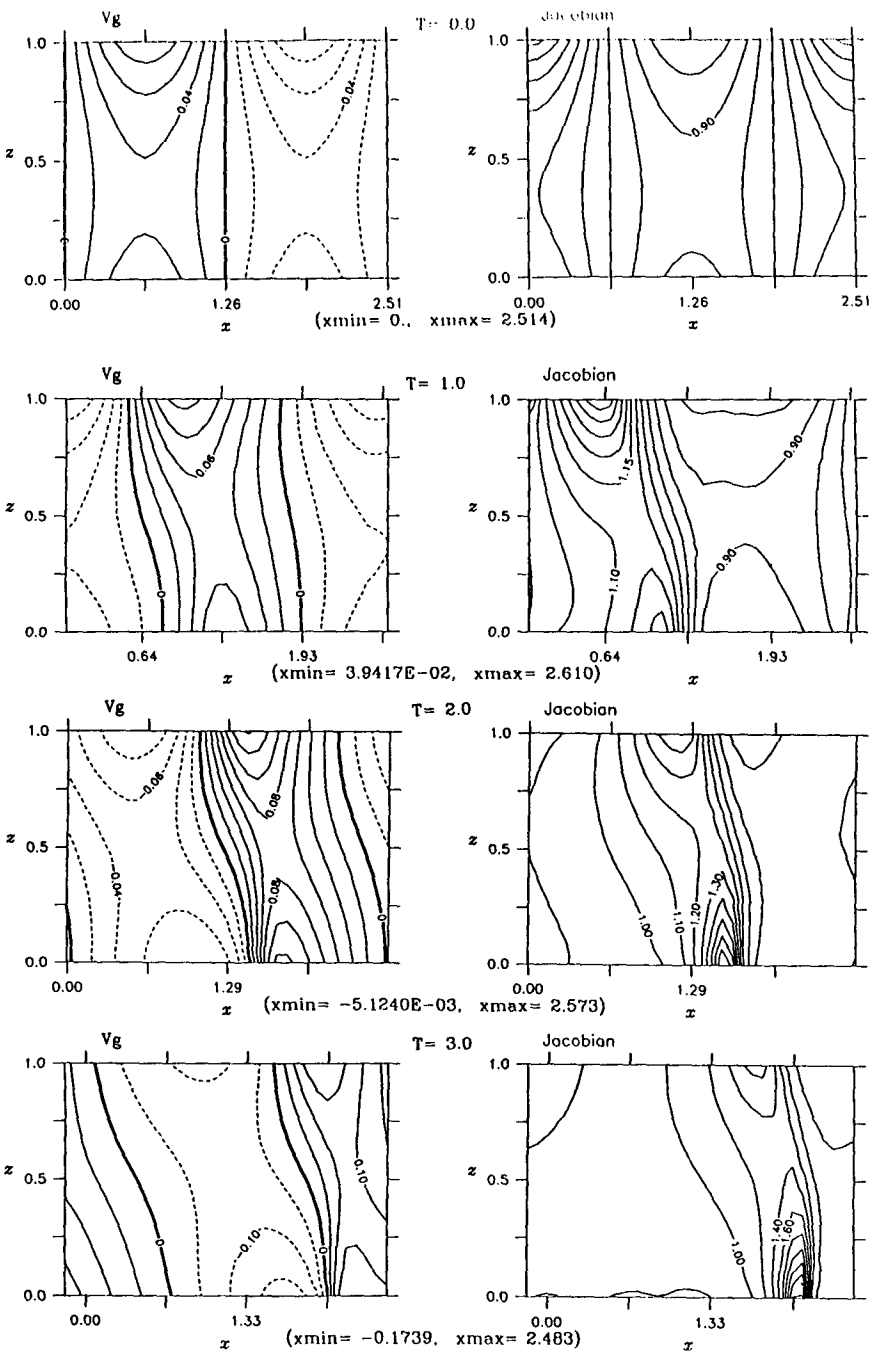


FIG. 2(a). Moist dynamics ($R = 0.01$) of the upper-dry neutral wave initial condition (3.1a) with a zonal wavenumber of $k = 2.5$. Shown are contour plots of the nondimensional $v_g$ and Jacobian fields at $T = 0$, 1, 2, and 3 nondimensional advection times with contour levels indicated on each plot. Note that the contour interval generally changes with time. A unit value of $v_g$ corresponds to 100 m s$^{-1}$. Solid lines denote positive values and dashed lines denote negative values. The minimum and maximum $x$ values are given in parentheses underneath each $v_g$ and Jacobian pair and these values change with time because of the geostrophic coordinate transformation $x = X - v_g(X, Z, T)$.

at the maximum of $\partial w/\partial z$ as $R_0 \to 0$. Since $\partial w/\partial z$ attains its maximum along $Z = 0$, the largest positive values of $q_g$ would be expected to occur along $Z = 0$. The figures confirm these conclusions both at early and later times with positive $q_g$ anomalies having their maxima along $Z = 0$.

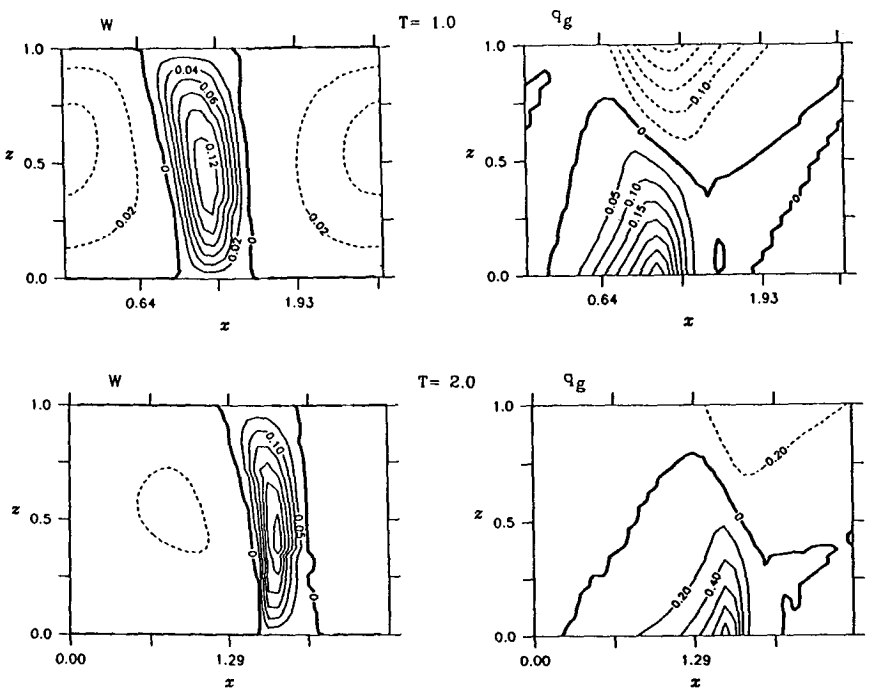


FIG. 2(b). Moist dynamics ($R = 0.01$) of the upper dry neutral wave initial condition (3.1a) with a zonal wavenumber of $k = 2.5$. Shown are contour plots of the nondimensional vertical velocity $w$ and anomalous dry potential vorticity $q_g$ at $T = 1$ and 2 nondimensional advection times with contour levels indicated on each plot. Note that the contour interval generally changes with time. A unit value of $w$ corresponds to 30 cm $s^{-1}$ and a unit value of $q_g$ corresponds to $10^{-4}$ $s^{-2}$ [($\approx 1/4$) PV units]. Solid lines denote positive values and dashed lines denote negative values. The minimum and maximum $x$ values for each time are the same as in Fig. 2a and are not listed.

After one advection time (dimensionally 9.25 h) the positive anomaly has a nondimensional maximum of 0.35 while the minimum of the negative anomaly is $-0.25$. At $T = 2$ the maximum in $q_g$ is 1.0 and occurs along the lower boundary while the minimum of the negative anomaly is $-0.3$ and located at the model tropopause near $x = 1.7$. In this example $q_g$ is never less than $-1$, so both Eqs. (2.11c, 2.11d) remain elliptic throughout the integration. A spatial integration of the right-hand side of (2.11a) vanishes as it should since latent heating cannot create any net potential vorticity with a heating representation that vanishes on the horizontal boundaries. The discrete equivalent of this condition is confirmed for all of the results reported.

The configuration of the potential vorticity field $q_g$ is dipolar with the presence of the basic-state wind aloft tending to displace the negative potential vorticity anomaly downstream of the positive surface anomaly. This is evident in all of the $q_g$ contour plots except at the time of frontal collapse where the minimum of the negative anomaly is not large enough to show up in the figure. This perturbation structure transports heat poleward with interaction of the induced anomalies enhancing the conversion of potential energy to perturbation energy. The $v_g$ field at $T = 0$ shows some overlap of the upper and lower fields for this particular wavenumber, but without latent heat release this disturbance propagates eastward as a neutral normal mode with no change in its vertical structure and no surface development. Thus, latent heating induces a favorably configured potential vorticity couplet in the interior giving rise to positive correlation between the induced fields ($v_g, \theta$) thereby enhancing the baroclinic coupling between the upper and lower fields.

Further experimentations with this disturbance, using slightly larger $R_0$ values of 0.1 and 0.2 did not show sensitivity to the initial amplitude. This is consistent with the findings in EFT where moist surface frontogenesis was found for infinitesimal disturbances even for a limited range of wavenumbers slightly greater than the short-wave cutoff of the dry Eady problem. If on the other hand, a series of experiments were performed with increasing $R_0$, $0 < R_0 < 1$, a qualitative change in the solution is expected beyond some critical value of $R_c$ since for $R_0 > R_c$ the upper and lower fields would no longer phase lock. Instead, transient development would occur as the upper-level disturbance passes over the surface induced disturbance.

Baroclinic coupling between the upper and lower induced disturbance occurs provided the disturbance aloft produces strong southerly advection of the surface induced warm potential temperature anomaly, i.e.,

$$\overline{v_{g_{upper}}\theta_{surf}} > 0,$$

where the bar denotes a zonal average. For a given interior $q_g$ distribution and $\theta$ on the horizontal boundaries the interior distribution of $\theta$ and $v_g$ results from the solution of the elliptic partial differential equation (2.11c). The characteristic vertical length scale of the $v_g$ and $\theta$ fields is generally controlled by the decay scale of the Green's function for Eq. (2.11c) associated with a point source located in the physical domain. If we assume $q_g$ small compared to unity and adhere to zonally periodic flows then the nondimensional vertical length scale will be close to the nondimensionalized Rossby penetration depth of quasi-geostrophic theory, namely $R_d = 1/k$, where $k$ is a characteristic zonal wavenumber of the disturbance. When $q_g$ is O(1) and varies slowly on the length scale of the disturbance, the form of the penetration depth will change approximately to $R_d = k^{-1}(1 + q_g)^{-1/2}$ (recall that $1 + q_g$ is interpreted as an equivalent static stability in semi-geostrophy). Consequently this penetration depth will tend to be reduced in regions where $q_g$ is positive and increased in regions where $q_g$ is negative although the penetration depth is still predominantly controlled by the zonal wavenumber. When $q_g$ is O(1) and varies rapidly on the scale of the $v_g$ and $\theta$ fields there is no simple expression for this penetration depth, but from a physical point of view qualitatively similar conclusions are expected. In light of these considerations a much weaker interaction is expected between the upper and lower induced anomalies for small wavelength disturbances of the same form as Eq. (3.1a) with $q_g$ confined to equivalent delta contributions along the horizontal boundaries.

Inspection of the cross-frontal Eq. (2.11d) shows that if $R_0 \to 0$ in updraft regions the effective penetration depth for the $\psi$ equation is increased substantially. Even for very short wavelength upper-level disturbances with no initial interior potential vorticity, the vertical velocity will tend to extend throughout the atmosphere as $R_0 \to 0$. If the $w$ field extends to the earth's surface positive potential vorticity will be induced there in accord with Eq. (2.11a) and its possible coupling with the initial disturbance aloft cannot be ruled out. Furthermore, for disturbances with initially nonuniform interior potential vorticity, baroclinic communication between upper and lower fields will be greatly enhanced by the combined effect of the increased penetration depth of the $w$ field in ascent regions and interaction of interior potential vorticity anomalies.

Baroclinic conversion of available potential energy into wave energy is ultimately regulated by the geopotential $\Phi$ since the interior $\theta$ and $v_g$ fields are derived from it. The extent of overlap between induced surface fields and upper-level fields is controlled by the local $\Phi$ penetration depth. Interestingly, this penetration depth is not explicitly dependent upon moist processes whereas the $\psi$ penetration depth is. Hence moist processes, as formulated here, introduce an asymmetry in the balance Eqs. (2.11c, 2.11d) by only modifying the penetration depth for the $\psi$ equation. This effect is not captured by simple reduction of the effective vertical stability in both balance equations as some ad hoc moisture parameterizations would suggest. The dynamics of short-wave disturbances involves a subtle interplay between the $w$ field, induced potential vorticity anomalies, and their baroclinic interaction.

In the next example, the form of the initial condition is the same as (3.1a), but $k = 4$, $c_r = 0.7496$, and $Bk = 0.05/27$ corresponding to a dimensional wavelength of 1570 km. The dimensional field has tropospheric maxima of approximately 10 m s$^{-1}$ and 3°K for $v_g$ and $\theta$. Figures 3a,b summarize this experiment and the most interesting features are discussed in the following points.

### 4) MERIDIONAL WINDS

The initial $v_g$ field has a barotropic structure and is confined to upper levels with almost no surface signature. At $T = 2$ a slight westward tilt with height of the $v_g$ field is present with a small surface signature. Moderate surface development has taken place after $T = 3$ with a maximum surface northerly wind of 7 m s$^{-1}$. Development is gradual at later times with northerly wind surface maxima of approximately 8 m s$^{-1}$ at $T = 4$.

### 5) VERTICAL VELOCITY

At $T = 0$ the vertical velocity in the ascent branch (not shown) extends between the two rigid lids but the descending branch has a minimum near $x = 1$, $Z = 0.75$ with a shorter vertical decay scale than that of the ascending branch. The width of this ascent region is approximately one-third that of the descent region at the initial time. Integration was stopped at $T = 5$ at which time the decay scale for the ascending and descending branches are comparable, although the $x$-width of the ascent region is roughly one-quarter the width of the descending branch. The ascending vertical velocity increases from 0.25 cm s$^{-1}$ at $T = 0$ to approximately 9 cm s$^{-1}$ at $T = 5$.

### 6) POTENTIAL VORTICITY AND JACOBIAN

As in the first example the initial potential vorticity anomaly $q_g$ of this disturbance is identically zero. However, the generalized potential vorticity anomaly field consists primarily of delta function contributions in $\theta$ along the horizontal boundaries $Z = 0$, 1 although signature of the surface $\theta$ is small. After one advection time the deep intruding ascending motion induces a positive potential vorticity anomaly near the surface and a negative anomaly aloft. By $T = 3$ the induced

anomalies extend from the boundaries into the interior and contribute to the overlap of the induced $v_g$ and $\theta$ fields to produce a baroclinic signature. At later times the disturbance system remains vertically phase locked and development continues but at a slower rate in comparison with the first example. The region with a Jacobian significantly different from unity is initially confined to upper levels but after the induction and intrusion of the potential vorticity anomalies, the Jacobian becomes largest along the lower boundary consistent with an increased relative vorticity of $0.4f$ near $x = 1.4$ at $T = 5$.

For this type of short-wave disturbance ISD occurs only after the induced potential vorticity structures advect close enough to interact baroclinically. Thus, short-wave disturbances with nonuniform interior potential vorticity may give rise to stronger surface fronts than disturbances with initially uniform interior potential vorticity. For example, consider the initial condition given by

$$\Phi(X, Z; 0) = \Phi_0\{\exp[-D(1 - Z)] \sin(kX + \epsilon \exp[-DZ] \sin(kX - \pi)\} \quad (3.1b)$$

where $k = 4$, $D = -2.3$, $\Phi_0 = 0.025$, and $\epsilon = 0.4$. This initial condition represents an upper-level interior potential vorticity anomaly positioned one-half wavelength upwind of the surface $q_g$ seed field whose magnitude is $\epsilon$ relative to the upper disturbance. The amplitude of the lower seed $v_g$ field is approximately 20% of the upper $v_g$ field. Rapid surface development is found in this case. The results are shown in Figs. (4a,b) and salient features are discussed in the following.

### 7) Potential vorticity

Along the lower surface $\theta$ has the same sign as $q_g$ and their maxima also coincide. This property holds true at later times so, for discussions we focus on the $q_g$ field. From Fig. 4b, the initial potential vorticity has its maxima along the model tropopause and decays exponentially in the vertical with secondary maxima at the surface. The nondimensional tropospheric maximum is 0.4 at $x = 1.2$. Taking into account the periodic domain the upper anomaly is seen to be upstream of the positive surface anomaly located at $x = 0.4$. By $T = 1$ the upper-level anomaly has been advected to a position upwind above the surface anomaly. During their interaction the upper and lower fields merge together and the resultant positive $q_g$ field has an upshear tilt characteristic of baroclinic conversion from available potential energy to perturbation energy. By $T = 2$ the initially positive upper tropospheric anomaly has almost disappeared leaving behing a broad scale diabatically induced negative anomaly. The surface $q_g$ anomaly continues to intensify increasing from 0.65 to 5.01 between $T = 1$ and $T = 4$.

### 8) Meridional winds and Jacobian

The initial $v_g$ and $J$ fields have their maxima at the model tropopause with secondary maxima at the surface. The maximum in $v_g$ and $J$ is 9.5 m s$^{-1}$ and 1.6, respectively, corresponding to a relative vorticity of $0.6f$. Figure (4a) shows a substantial increase of meridional wind with $v_g$ at the surface increasing from 2 m s$^{-1}$ at $T = 0$ to 6 m s$^{-1}$, 15 m s$^{-1}$, and 19.6 m s$^{-1}$ at $T = 1$, 2, and 3, respectively. An upshear phase tilt indicating baroclinic conversion is evident from the $v_g$ fields. The initial Jacobian has two maxima located at the upper and lower surface with values of 1.6 and 1.4, respectively. At later times the surface maximum dominates with values of 2.55, 4.25, and 2.5 at $T = 2$, 3, and 4, respectively, corresponding to relative vorticities at the lower surface of $1.55f$, $3.25f$, and $1.5f$. At subsequent times the phase signature of the $v_g$ field becomes nearly vertical and remains so, in an apparent phase lock, suggesting conversion of available potential energy to perturbation energy has been suppressed. Longer time integrations show only slow intensification near the lower surface.

This example shows increased surface development for short wave disturbances with interior potential vorticity but also shows more: as $R \to 0$, latent heat release produces a modest surface frontal zone with a relative vorticity on the order of $f$ which does not completely collapse. What occurs instead is partial equilibration or slow intensification of the frontal zone with the entire system propagating eastward. It may be that this slowly intensifying phase-locked development is associated with an exponentially growing normal mode of the nonlinear moist model in the limit $R \to 0$, as discussed in the work of Joly and Thorpe (1989).

The partial equilibration process is investigated further by increasing the amplitude of $\epsilon$ in Eq. (3.1b) to 0.8. This yields a maximum in the surface $v_g$ seed field of 7 m s$^{-1}$. Integration with $R_0 = 0.01$ results in a surface front at $T = 1.6$ with maximum Jacobian of 50. Figure (5a) displays the initial $w$, $q_g$, $v_g$, and Jacobian fields for the increased seed field. Comparing these initial fields with the seed fields associated with $\epsilon = 0.4$, shows substantial increase in the surface disturbance magnitude. In particular, the surface $q_g$ anomaly extends upward to approximately $Z = 0.4$ and has a maximum of 0.25 whereas the original disturbance had a surface maximum in $q_g$ of 0.06 and decayed rapidly in the vertical. The reason for frontal collapse in this case is that the increased strength of the potential vorticity seed field increases the overlap between the upper and lower potential vorticity fields enhancing their baroclinic interaction. Figure 5b shows the $w$, $q_g$, $v_g$, and Jacobian fields at $T = 1.59$. The surface $v_g$ maximum is 18.6 m s$^{-1}$ with nearly 30 m s$^{-1}$ across the cyclonic vorticity shear zone. The surface maximum in $q_g$ and $J$ is 29 and 50, respectively, the relative vorticity is $49f$, and the maximum in the as-

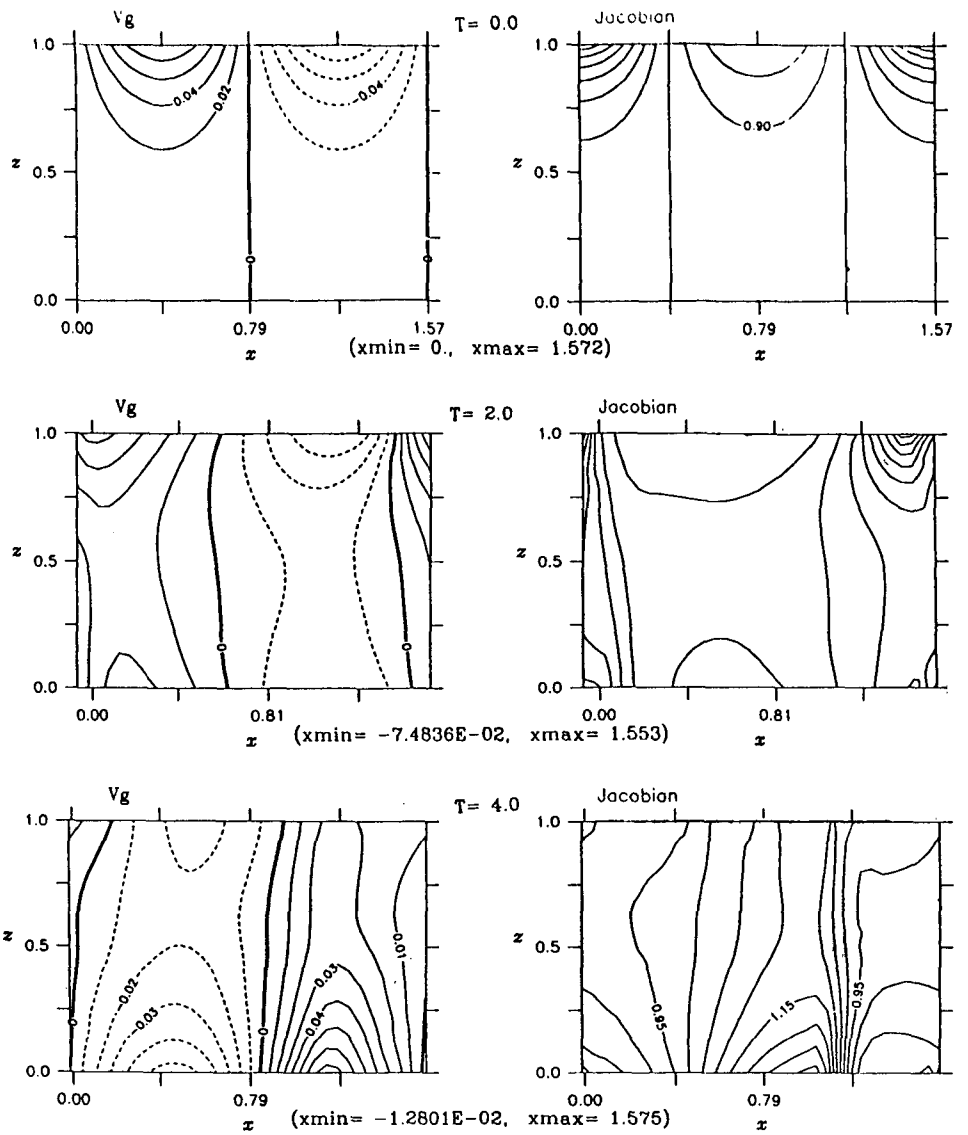


FIG. 3(a). Moist dynamics ($R = 0.01$) of the upper dry neutral wave initial condition (3.1a) except with a zonal wavenumber of $k = 4$. Shown are contour plots of the nondimensional $v_g$ and Jacobian fields at $T = 0$, 2, and 4 nondimensional advection times with contour levels indicated on each plot. Note that the contour intervals generally change with time and the plotting convention is the same as in Fig. 2.

cending velocity is 37.5 cm $s^{-1}$. In this case partial equilibration is suppressed by increased surface disturbances. Similar results hold if the strength of the upper-level disturbance is raised. Hence, strong disturbances rapidly produce collapsed surface fronts while weak disturbances develop more slowly and produce partially equilibrated or slowly intensifying structures.

We next increase $R_0$ from 0.01 to 0.3 and initialize the integration with (3.1b). The results of this experiment are summarized in Fig. 6 where the $v_g$ and $q_g$ fields are shown at $T = 1$ and $T = 3$. In contrast to the first case with $R_0 = 0.01$, the integration shows very weak surface development, and the structure no longer remains phase locked but rather the upper disturbance passes over the surface disturbance. Since the rate of induction of dry potential vorticity $Q_{g_0} = 1 + q_g$ decreases with increasing $R_0$, the magnitude of $q_g$ should be smaller in this case than the first. A comparison of the Figs. 6 and 4b confirms this property with a $q_g$ surface maximum of 0.4 at $T = 3$ for the current run compared to a maximum of 2.91 for the first run with $R_0 = 0.01$.

For the last experiment of this section we take the moist stability distribution (2.10b) with $R_0 = 0.01$ and again initialize the integration with (3.1b). Figure 7 shows the resulting $v_g$ and $q_g$ fields at $T = 1$ and $T = 3$. Limiting the extent of the moist neutral region inhibits

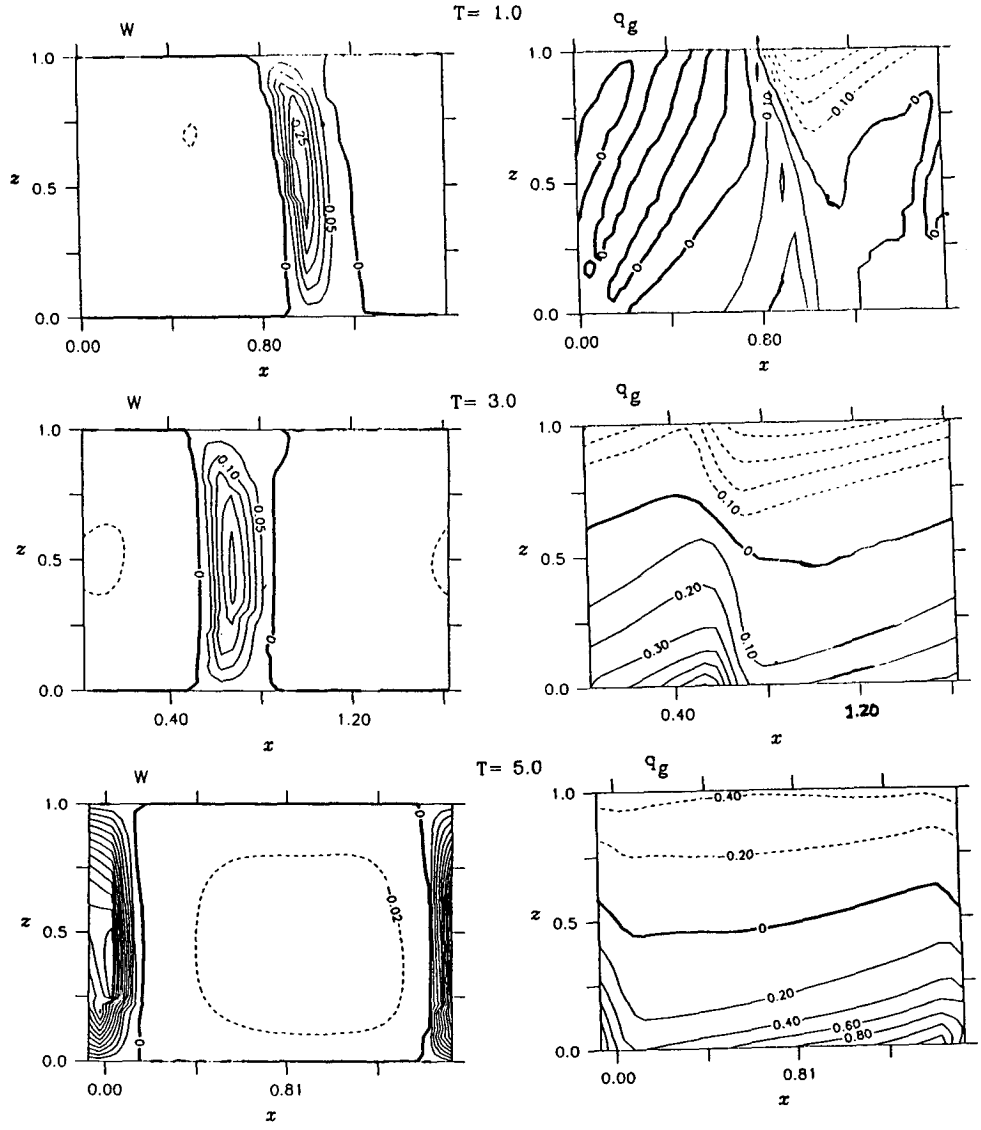


FIG. 3(b). Moist dynamics ($R = 0.01$) of the upper dry neutral wave initial condition (3.1a) except with a zonal wavenumber of $k = 4$. Shown are contour plots of the nondimensional vertical velocity $w$ and anomalous dry potential vorticity $q_g$ at $T = 1$, 3, and 5 nondimensional advection times with contour levels indicated on each plot. Note that the contour interval generally changes with time and the plotting convention is the same as in Fig. 2. The contour interval for $w$ is 0.05. The minimum and maximum $x$ values are approximately the same as in Fig. 3a.

the generation of surface potential vorticity and suppresses baroclinic coupling between the upper disturbance and surface anomaly. As in the preceding example, the upper disturbance does not phase lock with the surface disturbance.

Summarizing, disturbances with strong interior potential vorticity result in rapid surface frontogenesis in regions of deep near moist neutrality. With moderate moist stability or with vertically limited moist neutrality, the upper disturbance induces weak surface development and passes over the surface potential vorticity anomaly.

### *b. Diabatic destabilization of neutral surface waves*

We have illustrated the dynamics of induced low-level potential vorticity in the case of forcing by upper-level short wavelength potential vorticity disturbances. However, diabatic induction of potential vorticity is a more general phenomenon and does not arise solely from upper-level forcing. Further insight into the role of potential vorticity induction in surface processes is obtained by considering a class of flows with surface concentrated dynamics. The dynamics will remain surface concentrated provided we choose:

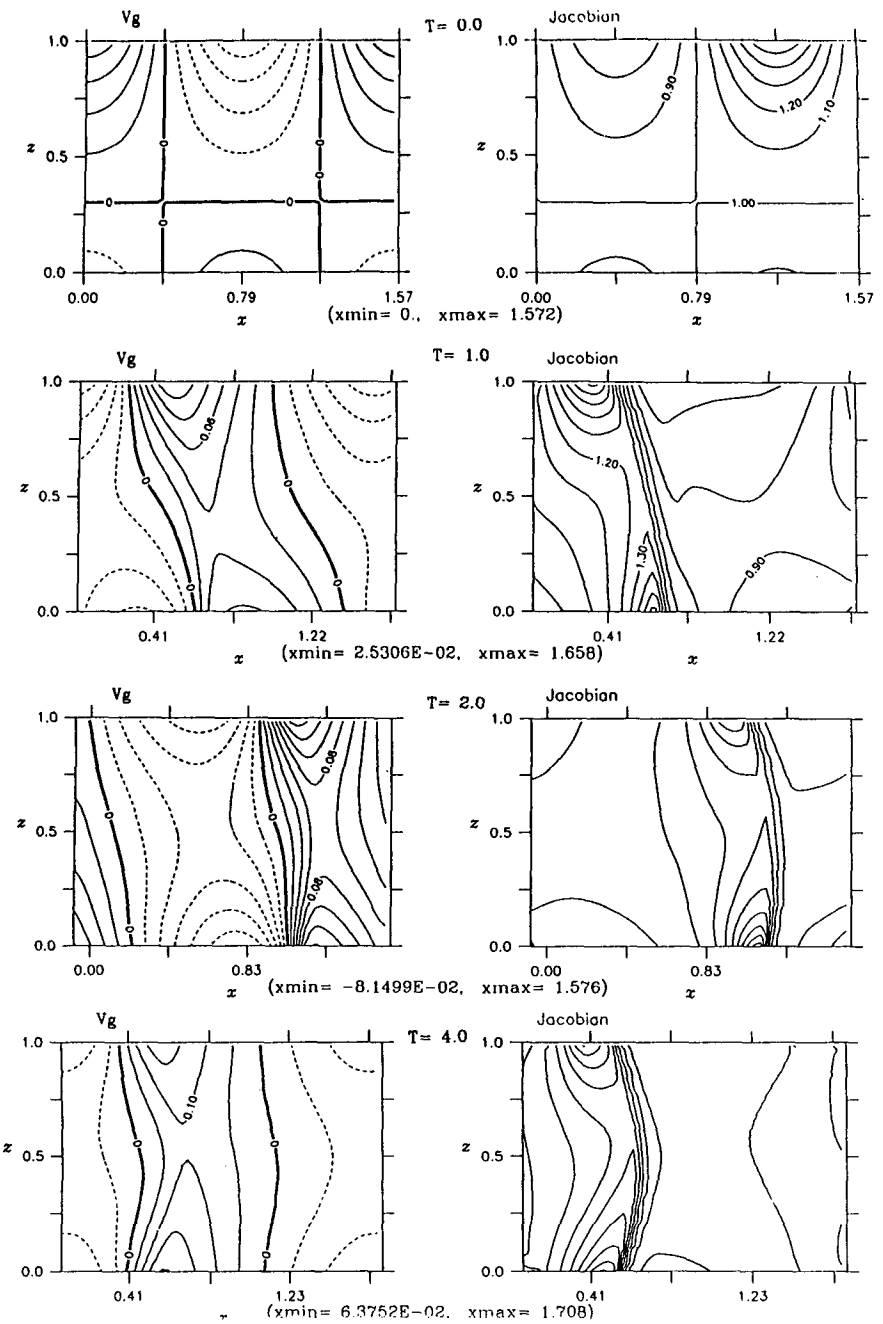


FIG. 4(a). Moist dynamics of the initial condition (3.1b) with a zonal wavenumber of $k = 4$, $\epsilon = 0.4$, and an $R$ value of 0.01. Shown are contour plots of the nondimensional $v_g$ and Jacobian fields at $T = 0$, 1, 2, and 4 nondimensional advection times with contour levels indicated on each plot. Note that the contour interval generally changes with time and the plotting convention is the same as in Fig. 2. The contour interval for the Jacobian at $T = 0$, 1 is 0.10 and changes to 0.20 for $T = 2$, 4.

1) an $R(Z)$ profile that inhibits induction of potential vorticity at higher levels near the tropopause and physically corresponds to a decreased latent heating in the vertical,

2) short wavelength perturbations as initial conditions having their maxima along $Z = 0$ to prevent significant penetration of fields aloft.

The first condition is met for an $R$ profile of the form (2.10b) increasing linearly with height and sat-

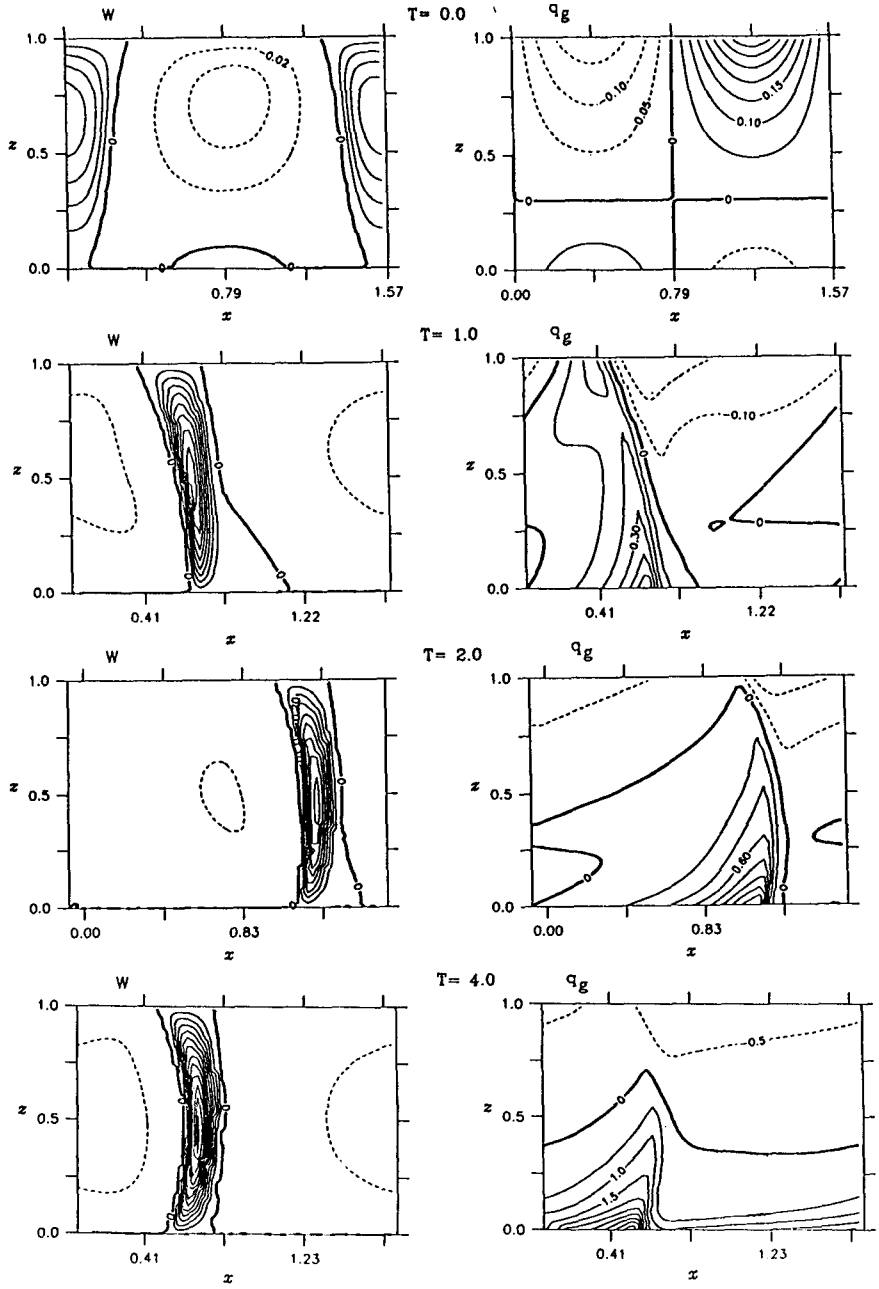


FIG. 4(b). Moist dynamics of the initial condition (3.1b) with a zonal wavenumber of $k = 4$, $\epsilon = 0.4$, and an $R$ value of 0.01. Shown are contour plots of the nondimensional vertical velocity $w$ and the anomalous dry potential vorticity $q_g$ at $T = 0$, 1, 2, and 4 nondimensional advection times with contour levels indicated on each plot. Note that the contour interval generally changes with time and the plotting convention is the same as in Fig. 2. The contour interval for $w$ at $T = 0$ is 0.02 and changes to 0.10 for $T = 1$, 2, 4.

isfying $R = R_0$ at $Z = 0$, and $R = 1$ at $Z = 1$. A dry neutral lower Eady mode with $k = 4$ satisfies the second condition

$$\Phi(X, Z; 0) = \mathrm{Re}\{[A \cosh(kZ) + B \sinh(kZ)] \exp(ikX)\} \quad (3.2)$$

where $Bk = 2/27$, $c_r = 0.2503$, $A/B = -kc_r$. Dimensional values for this perturbation are a maximum meridional surface wind of 7.3 m s$^{-1}$ and a maximum surface temperature perturbation of 2.5°K. Features of this simulation for $R_0 = 0.01$ are shown in Fig. (8a,b) and discussed further in text.

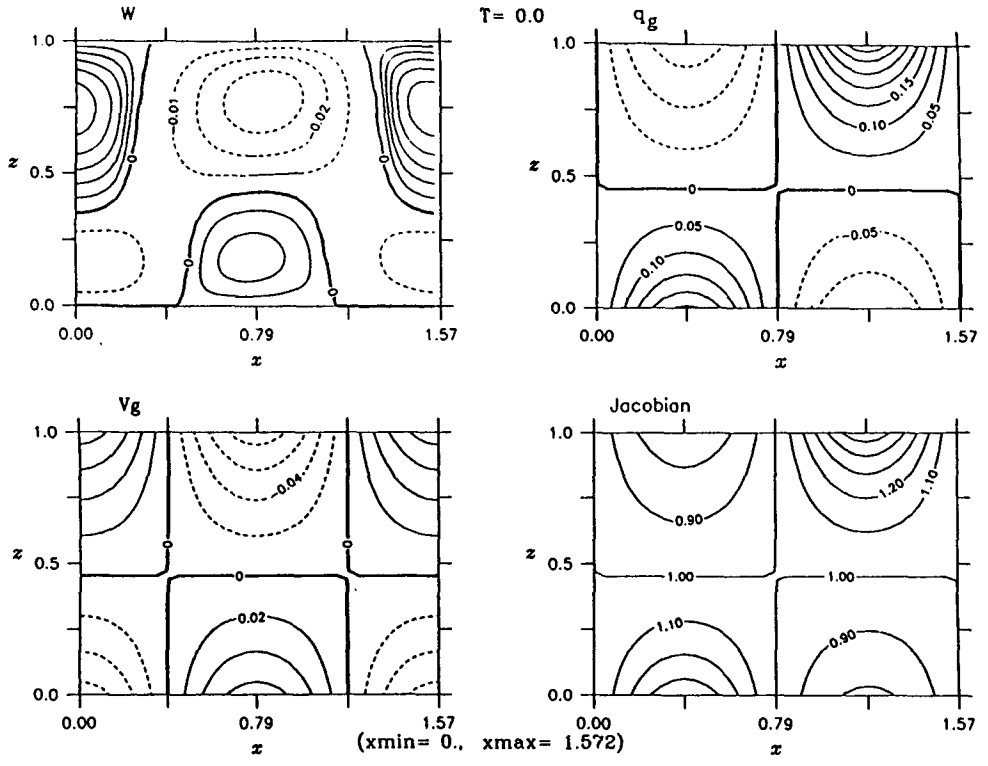


FIG. 5(a). Structure of the initial condition (3.1b) with a zonal wavenumber of $k = 4$, but with twice the amplitude of the lower seed field, i.e., $\epsilon = 0.8$. Shown are contour plots of the nondimensional vertical velocity, $w$, anomalous dry potential vorticity, $q_g$, meridional velocity $v_g$, and Jacobian field with contour levels indicated on each plot. Solid lines denote positive values and dashed lines denote negative values. The minimum and maximum $x$ values are given in parentheses.

### 1) POTENTIAL VORTICITY

Initially the generalized potential vorticity perturbation is confined to the surface $Z = 0$ in the form of a delta function in $\theta$ as discussed in the previous section. The interior potential vorticity anomaly $q_g$ is identically zero. At $T = 1$ a positive near surface anomaly and a negative interior anomaly located above and slightly eastward of the positive anomaly have been induced. The dipolar potential vorticity configuration results in a poleward heat transport converting available potential energy into perturbation energy. The westward tilt with height of the meridional wind field $v_g$ provides evidence of baroclinic conversion as the disturbance amplifies. The nondimensional positive anomaly increases in magnitude to 0.49, 1.17, and 2.97 at $T = 1$, 2, and 4, respectively while the negative anomaly increases in magnitude much more slowly with a minimum of $-0.26$ at $T = 4$. As the surface development proceeds the positive potential vorticity anomaly is advected away from the ascending region.

### 2) MERIDIONAL WINDS AND JACOBIAN

The initial fields have a barotropic structure with a surface maximum in meridional wind and Jacobian of 7.3 m s$^{-1}$ and 1.5. The maximum relative vorticity is $0.5f$. The maximum of $v_g$ occurs along the lower surface at all times and at $T = 4$ shows a negligible tropospheric signature but an increased signature at midlevels due to the induced interior potential vorticity there. The $v_g$ field displays a gradual increase in time with a maximum in $v_g$ of 7.8, 9.27, and 10.9 m s$^{-1}$ at $T = 1$, 2, and 4, respectively, and continued increase at later times. The maximum of the Jacobian occurs on the lower boundary and is 1.33, 1.49, 2.03 at $T = 1$, 2, and 4 with corresponding relative vorticities of $0.33f$, $0.49f$, $1.03f$ respectively. At $T = 4$ the beginning of frontal collapse in the $q_g$, $v_g$ and Jacobian fields is seen with an increased gradient across the cyclonic vorticity region. Since the rate of baroclinic development is proportional to the westward tilt of the disturbance, the slight westward tilt of the $v_g$ field with height implies a small growth rate, and this is consistent with the computational results. In contrast with the first class of examples, which showed rapid surface development, this disturbance intensifies much more slowly.

### 3) VERTICAL VELOCITY

The initial vertical velocity has nearly the same maximum and minimum of approximately 1 cm s$^{-1}$

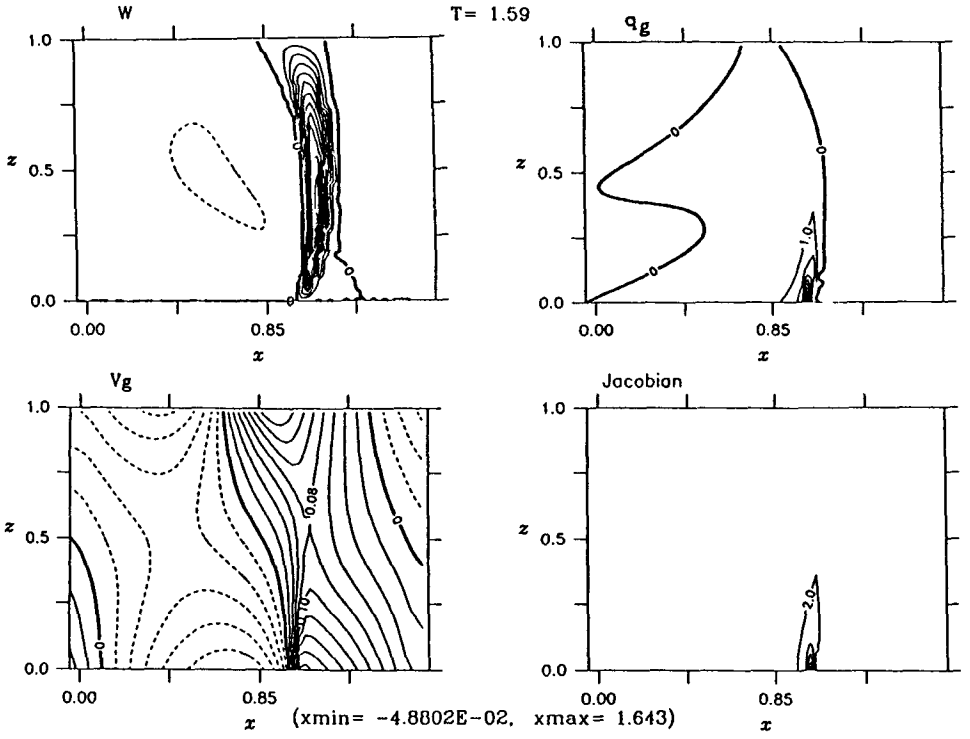


FIG. 5(b). Resultant fields with moist ($R = 0.01$) dynamics at 1.59 nondimensional advection times for the initial disturbance of (a). Shown are contour plots of the nondimensional vertical velocity, $w$, anomalous dry potential vorticity $q_g$, meridional velocity $v_g$, and Jacobian field with contour levels indicated on each plot. The contour interval for $w$ is 0.10. The minimum and maximum $x$ values are different from (a) because of the geostrophic coordinate transformation $x = X - v_g(X, Z, T)$.

and the ascent and descent regions exhibit almost identical decay scales. At $T = 2$ the width of the ascent region is half the width of the descent region with an approximate maximum ascent velocity of 1.9 cm $s^{-1}$, twice the absolute minimum velocity of the descent region. The linear increase of $R(Z)$ to unity at $Z = 1$ results in an attenuation of the ascending vertical velocity at upper levels that would have resulted in the uniform small $R$ case. Thus, the upward velocity decay scale is shorter for the case (2.10b) than (2.10a) implying more limited ascending regions. At $T = 2$, and $T = 4$ the vertical decay scale of the upward velocity is shorter than the decay scale of the downward velocity. The location of the maximum surface induced interior potential vorticity, $q_g$, occurs within the ascent region but inspection of the figures shows that the surface $q_g$ maxima is slightly west of the vertical velocity maximum. The maxima in $w$ at $T = 4$ is 2.5 and $-1.2$ cm $s^{-1}$ for the ascending and descending velocities, respectively. This disturbance generates $w$ maxima that are weaker than examples in the previous section.

The lower-level disturbance (3.2) develops more slowly than the deep disturbances of the first section. Nevertheless, a surface front does form in finite time. To make longer integrations reliable the quasi-static approximation for $R(Z)$ is discarded and (2.8) is explicitly integrated with the initial condition $S_e(X, Z, 0) = \Gamma_d R(Z)/\Gamma_m$ and $\Gamma_d/\Gamma_m = 1$. At $T = 6.8$ a strong surface front forms with maxima in relative vorticity of $21.1f$ and vertical velocity of 12.5 cm $s^{-1}$. If the amplitude of the initial condition (3.2) is halved the maximum in $v_g$ is reduced to 3 m $s^{-1}$. Figure 9 shows the result of this integration at successive times. In this case a strong surface front forms at $T = 11.4$ with a maximum relative vorticity of $19f$ and a vertical velocity maximum of 13 cm $s^{-1}$. Doubling the amplitude of the initial condition (3.2) yields a surface front at $T = 2.6$ with maxima in relative vorticity, northerly surface winds, and vertical velocity of $50f$, 23 m $s^{-1}$, and 13 cm $s^{-1}$, respectively. The results of these three experiments are summarized in Table 2 where surface maxima for $v_g$, $q_g$, and $J$ are recorded at various times. In general, the time of frontal formation varies inversely with the strength of the initial disturbance and despite the initially slow growth of these disturbances a surface front eventually forms regardless of the initial strength.

If $R \equiv 1$ in (2.11, 2.12) the system reduces to the dry semigeostrophic system of previous work (Montgomery and Farrell 1990). That work demonstrated the existence of an amplitude threshold for short wave perturbations: strong disturbances that exceed this threshold develop surface fronts whereas weak distur-

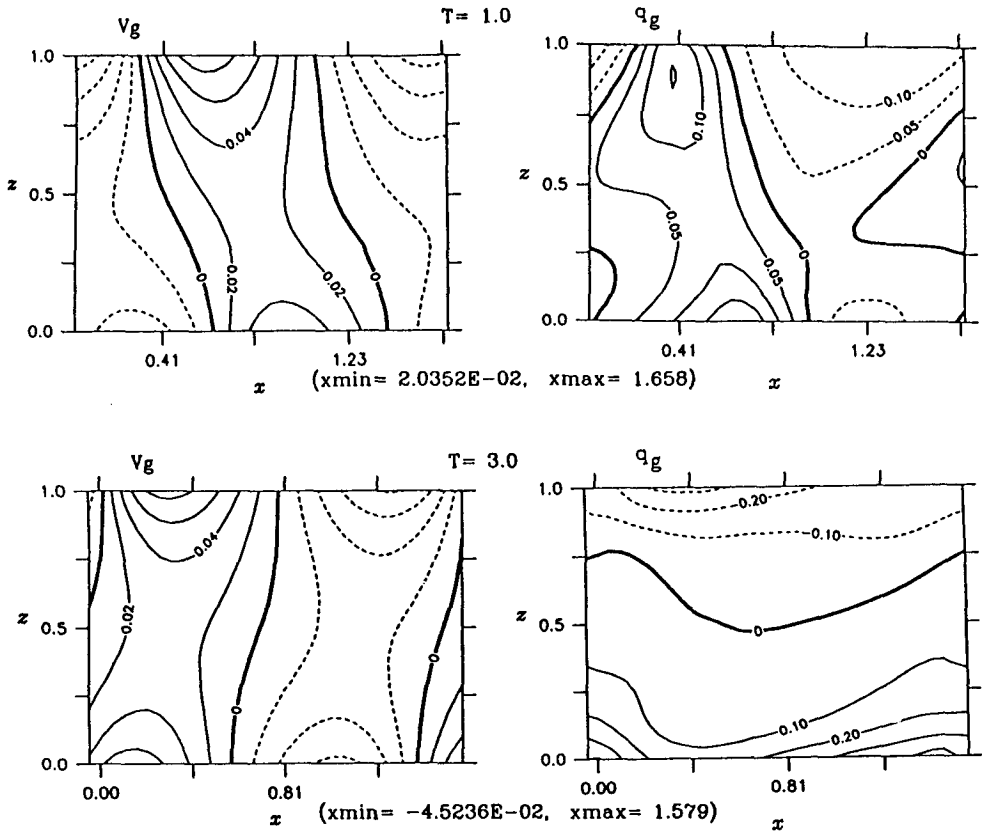


FIG. 6. Moist dynamics of the initial condition (3.1b) with a zonal wavenumber of $k = 4$, $\epsilon = 0.4$, but an increased $R$ parameter of 0.3. Shown are contour plots of the nondimensional meridional velocity $v_g$ and anomalous dry potential vorticity $q_g$ at $T = 1$, and 3 nondimensional advection times with contour levels indicated on each plot. Note that the contour interval generally changes with time and the plotting convention is the same as in Fig. 2.

bances do not. In light of this it may seem surprising that the moist model (2.11) does not possess a similar amplitude threshold for short-wave disturbances such as (3.2). Table 2 displays the maxima of $q_g$, $v_g$, $J$, and $w$ for the three cases discussed above at various times and the salient feature is the continual increase in $v_g$, $q_g$, and $w$ with time. From previous considerations regarding the local $\Phi$ penetration depth $R_{pen}$, the generation of large positive $q_g$ along the lower surface implies a reduction of $R_{pen}$ in these regions. A decrease in $R_{pen}$ suppresses baroclinic interaction between the induced surface potential vorticity anomaly and the downstream anomaly. This suggests weak surface development at later times. However, the results of Table 2 show monotonic surface development and do not show magnitudes that level off with time. Clearly, the baroclinicity of the background state is not the only source of energy for the disturbance. The physical reason for this development is revealed by examining the (dimensional) Eq. (2.4e) for the cross-frontal streamfunction $\psi$:

$$\frac{\partial}{\partial X}\left(Q_{g_{\text{eff}}}\frac{\partial \psi}{\partial X}\right) + f^2\frac{\partial^2 \psi}{\partial Z^2} = -2fS\frac{\partial v_g}{\partial X} = -2\frac{\partial v_g}{\partial X}\frac{g}{\theta_0}\frac{\partial \bar{\theta}}{\partial Y}, \quad (3.3)$$

where thermal wind balance of the basic state was used in the last expression. If the background meridional temperature gradient $\partial\bar{\theta}/\partial Y$ is zero the only physically admissible solution for $Q_{g_{\text{eff}}} > 0$ is $\psi \equiv 0$ and hence $w \equiv 0$. Conversion of latent heat energy to perturbation energy is impossible without ascending motion. Alternatively, when $\partial\bar{\theta}/\partial Y \neq 0$ a nonzero vertical velocity field is required for any disturbance with $\partial v_g/\partial X \neq 0$ in order to maintain thermal wind balance. In this case there is conversion of latent energy into perturbation energy in ascent regions. In fact in the $R \to 0$ limit, the dry potential temperature equation implies that ascending motion cannot change the thermal structure. Hence, almost all of the induced potential vorticity goes directly into relative vorticity $\partial v_g/\partial X$. Increased

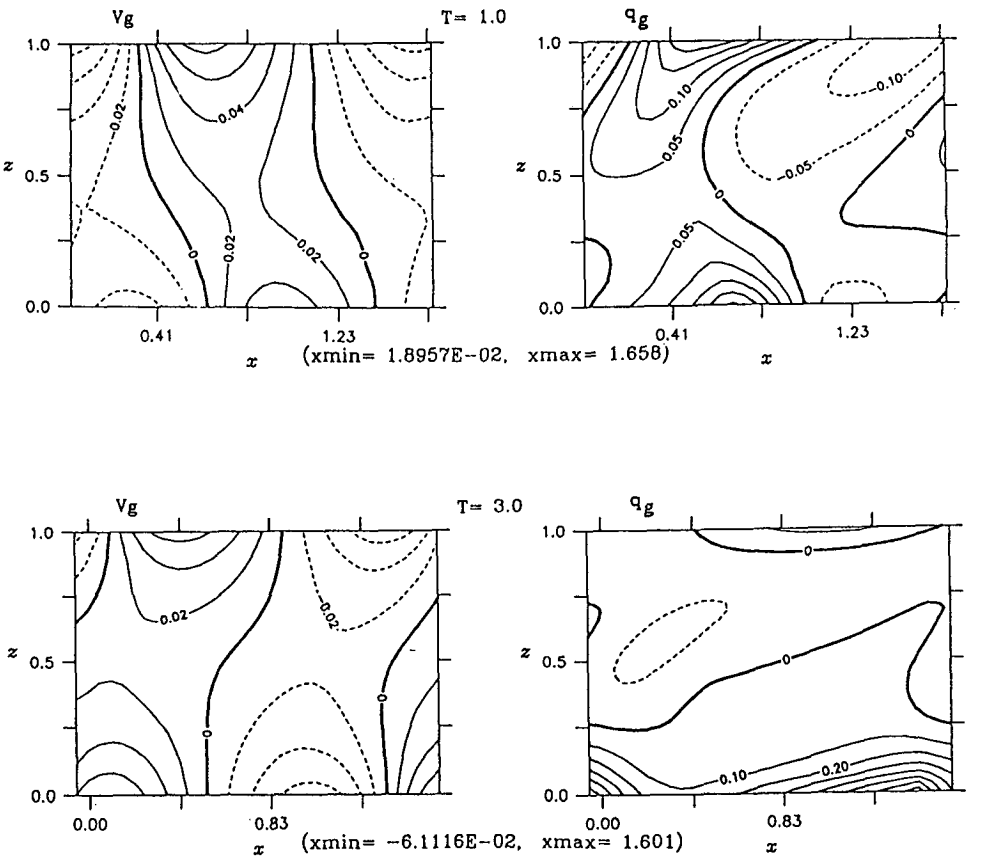


FIG. 7. Moist dynamics of the initial condition (3.1b) with a zonal wavenumber of $k = 4$, $\epsilon = 0.4$, and a moist stability distribution $R(Z) = R_0 + (1 - R_0)Z$, with $R_0 = 0.01$. Shown are contour plots of the nondimensional meridional velocity $v_g$ and anomalous dry potential vorticity $q_g$ at $T = 1$, and 3 nondimensional advection times with contour levels indicated on each plot. Note that the contour interval generally changes with time and the plotting convention is the same as in Fig. 2.

relative vorticity along the lower surface results in an increase in meridional winds $v_g$ and hence increased disturbance kinetic energy. Thus, although this process is not primarily driven by baroclinic energetics it is crucially dependent on a background baroclinic environment. Without a baroclinic background state such moist surface development is not possible.

When we increase $R_0$ from 0.01 to 0.2 for the disturbance (3.2) or increase the wavenumber to $K = 6$, surface development is found with a surface front forming in finite time. It is thus evident that surface development for this class of disturbances is robust and not dependent upon the initial amplitude of the disturbance, the zonal wavelength, or the magnitude of $R_0$.

## 4. Discussion and conclusion

We have investigated moist surface frontogenesis associated with initial disturbances of short wavelength with both uniform and nonuniform potential vorticity using a semigeostrophic model, which incorporates vertical temperature dependence in the heating term giving correct asymptotic behavior at high and low temperatures. Two flow classes of principal physical interest occur when the parameter $R$, interpreted here as the deviation from moist neutrality, is either small and uniform or a monotonic increasing function of height. These cases correspond to a deep and surface confined near-moist neutral region, respectively. For short wavelength disturbances latent heat release is shown to result in new frontogenetic processes for both classes of flows.

For the first class, examples delineate critical factors in the interaction between preexisting upper-level potential vorticity anomalies and diabatically induced potential vorticity at the lower surface. Moist dynamics associated with the passage of an upper-level disturbance over a surface disturbance proceeds in two stages. In the induction phase, the upward velocity field downstream of the upper disturbance extends vertically through the atmosphere and, as $R \to 0$ induces positive

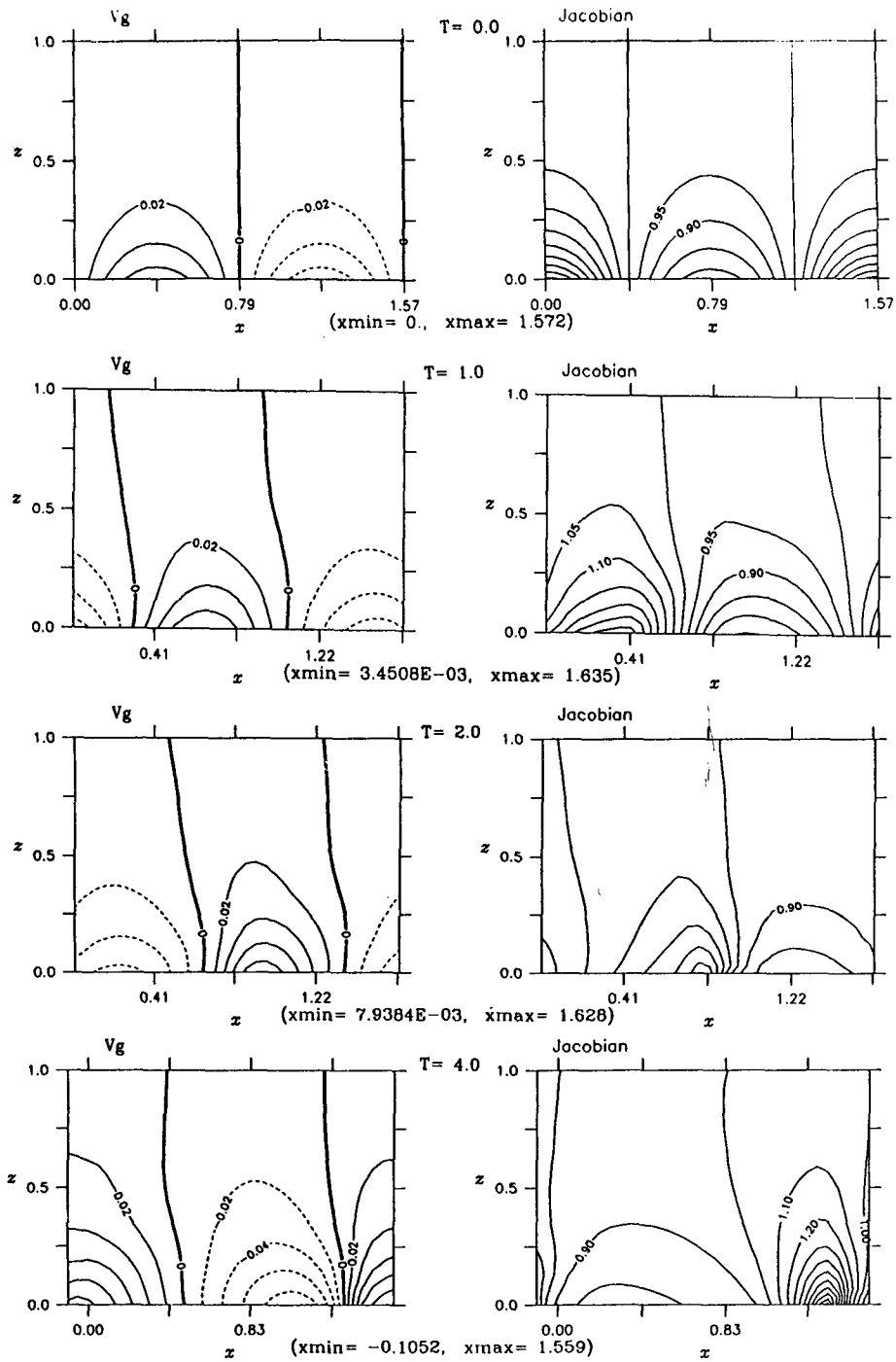


FIG. 8(a). Moist dynamics of the lower dry neutral wave initial condition (3.2) with a zonal wavenumber of $k = 4$, $R(Z) = R_0 + (1 - R_0)Z$, and $R_0 = 0.01$. Shown are contour plots of the nondimensional $v_g$ and Jacobian fields at $T = 0$, 1, 2, and 4 nondimensional advection times with contour levels indicated on each plot. Note that the contour interval generally changes with time and the plotting convention is the same as in Fig. 2.

potential vorticity near the surface. In the interaction phase, baroclinic coupling occurs between the disturbance aloft and the induced potential vorticity near the lower surface. Baroclinic conversion from basic-state available potential energy to disturbance energy is principally controlled by the relationship between the anomalous potential vorticity $q_g$ and geopotential $\Phi$. However, since moist processes are not explicit in

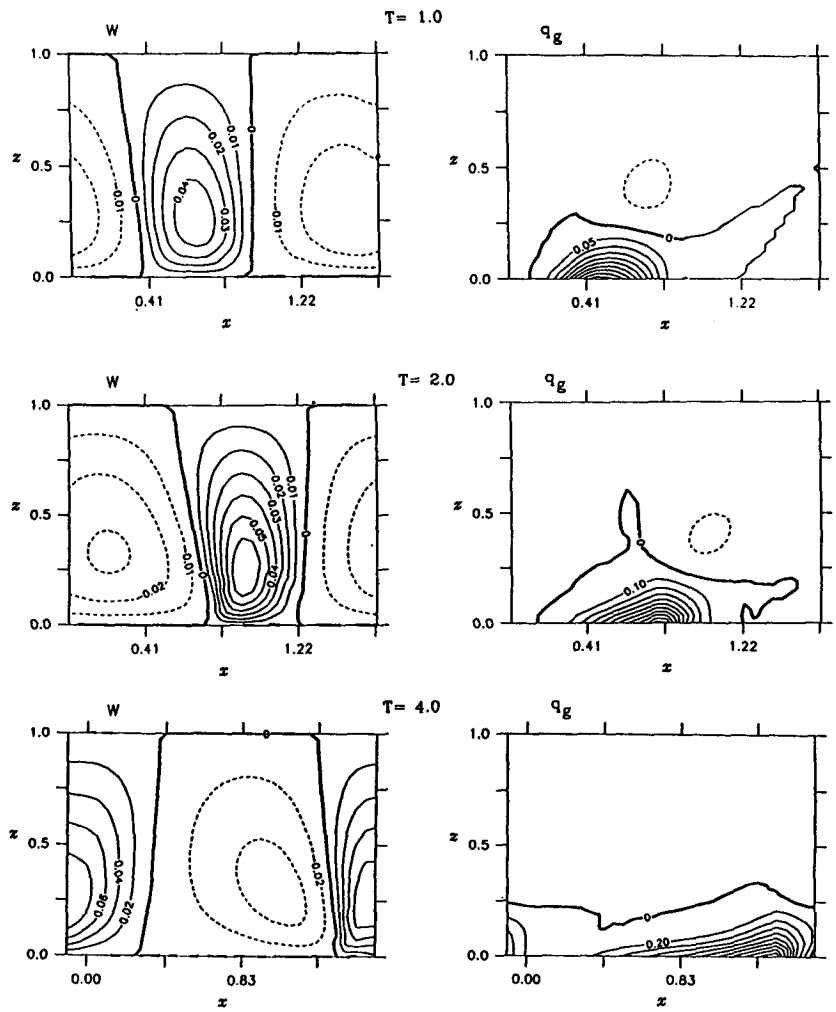


FIG. 8(b). Moist dynamics of the lower dry neutral wave initial condition (3.2) with a zonal wavenumber of $k = 4$, $R(Z) = R_0 + (1 - R_0)Z$, and $R_0 = 0.01$. Shown are contour plots of the nondimensional vertical velocity $w$ and dry anomalous potential vorticity $q_g$ at $T = 1$, 2, and 4 nondimensional advection times with contour levels indicated on each plot. Note that the contour interval generally changes with time and the plotting convention is the same as in Fig. 2.

this relation, the form of the local Rossby penetration depth is unchanged and formally identical to the penetration depth of the complimentary dry system obtained by setting $R \equiv 1$. Consequently, upper- and lower-level disturbances of short wavelength with uniform potential vorticity are generally less likely to couple baroclinically than similar long-wave disturbances: short-wave disturbances aloft induce only a small poleward heat transport at the surface. In contrast, coupling can be strong for short-wave disturbances with nonuniform potential vorticity in the interior; the potential vorticity is no longer confined to delta functions in $\theta$ on the horizontal boundaries $Z = 0$, 1 as in the uniform potential vorticity case. With interior potential vorticity and a value of $R = 0.01$ rapid surface frontogenesis during the interaction of a strong upper disturbance is found with $v_g$ maximum of 9.5 m s$^{-1}$ and a surface disturbance with $v_g$ maximum of 6 m s$^{-1}$. Also, we find a partially equilibrated or slowly intensifying surface frontal zone for a similar initial condition but with half the original magnitude at the surface. After an initial transient adjustment period these solutions appear to be phase locked. For $R$ uniformly equal to 0.3 and for $R$ increasing linearly with height the same upper-level vorticity disturbance no longer phase locks with the induced surface potential vorticity. In these examples surface development is weak as the upper disturbance is advected over the surface disturbance. For this first class of flows it is concluded that rapid surface frontogenesis occurs only with a combination of interior potential vorticity anomalies and deep moist neutrality.

Using the second class of flows we investigate the moist dynamics associated with induction of surface

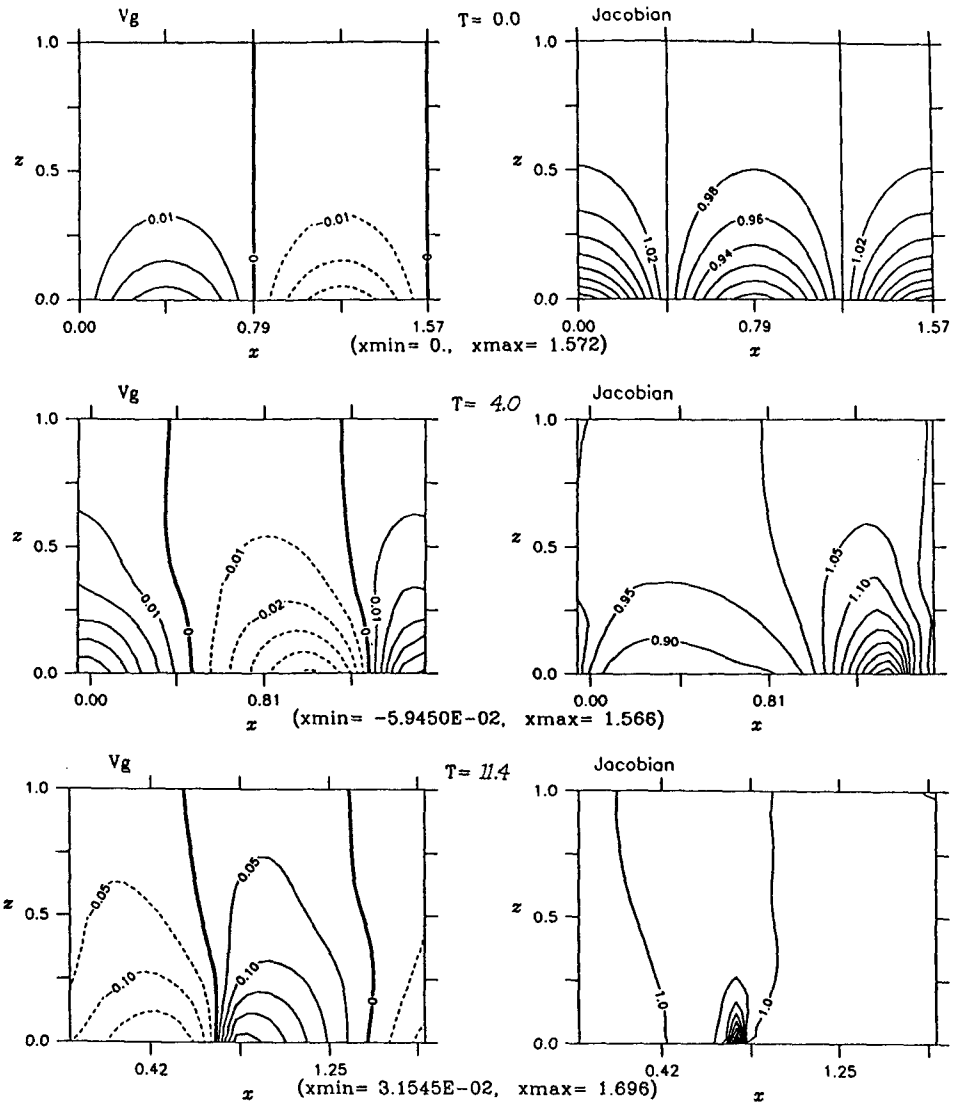


FIG. 9. Moist dynamics of the initial condition (3.2) with a zonal wavenumber of $k = 4$, $R(Z) = 0.01 + (1 - 0.01)Z$, but at half the initial amplitude of Fig. 7(a). Shown are contour plots of the nondimensional $v_g$ and Jacobian fields at $T = 0$, 4, and 11.44 nondimensional advection times with contour levels indicated on each plot. Note that the contour interval generally changes with time and the plotting convention is the same as in Fig. 2. The maximum of the Jacobian at 11.44 advection times is 20 corresponding to a relative vorticity of $19f$.

potential vorticity observed in the first class discussed above. Diabatic influences near the upper boundary are eliminated if the moist stability function $R(Z)$ increases linearly with height and equals unity along the upper boundary: $R(Z) = R_0 + (1 - R_0)Z$.

We consider initial disturbances that are neutral normal modes having wavenumbers much greater than the short-wave cutoff of the dry Eady problem. Latent heat release is shown to destabilize these disturbances. Initially, destabilization occurs through induction of a negative interior potential vorticity anomaly downstream of the surface induced positive anomaly: the spatial configuration of the vorticity couplet transports heat poleward and increases the disturbance kinetic energy. At later times the increase of the surface potential vorticity reduces the local penetration depth of the $\Phi$ equation tending to weaken baroclinic interaction between the potential vorticity anomalies. However, maintenance of thermal wind balance in a baroclinic environment requires a nonzero vertical velocity field and, hence, release of latent heat in ascending regions. The latent heat release induces dry potential vorticity in the interior and as $R \to 0$ the increased potential vorticity is manifest as an increase of surface winds. The disturbance continues to grow at later times and frontal collapse occurs in a finite time. For similar dis-

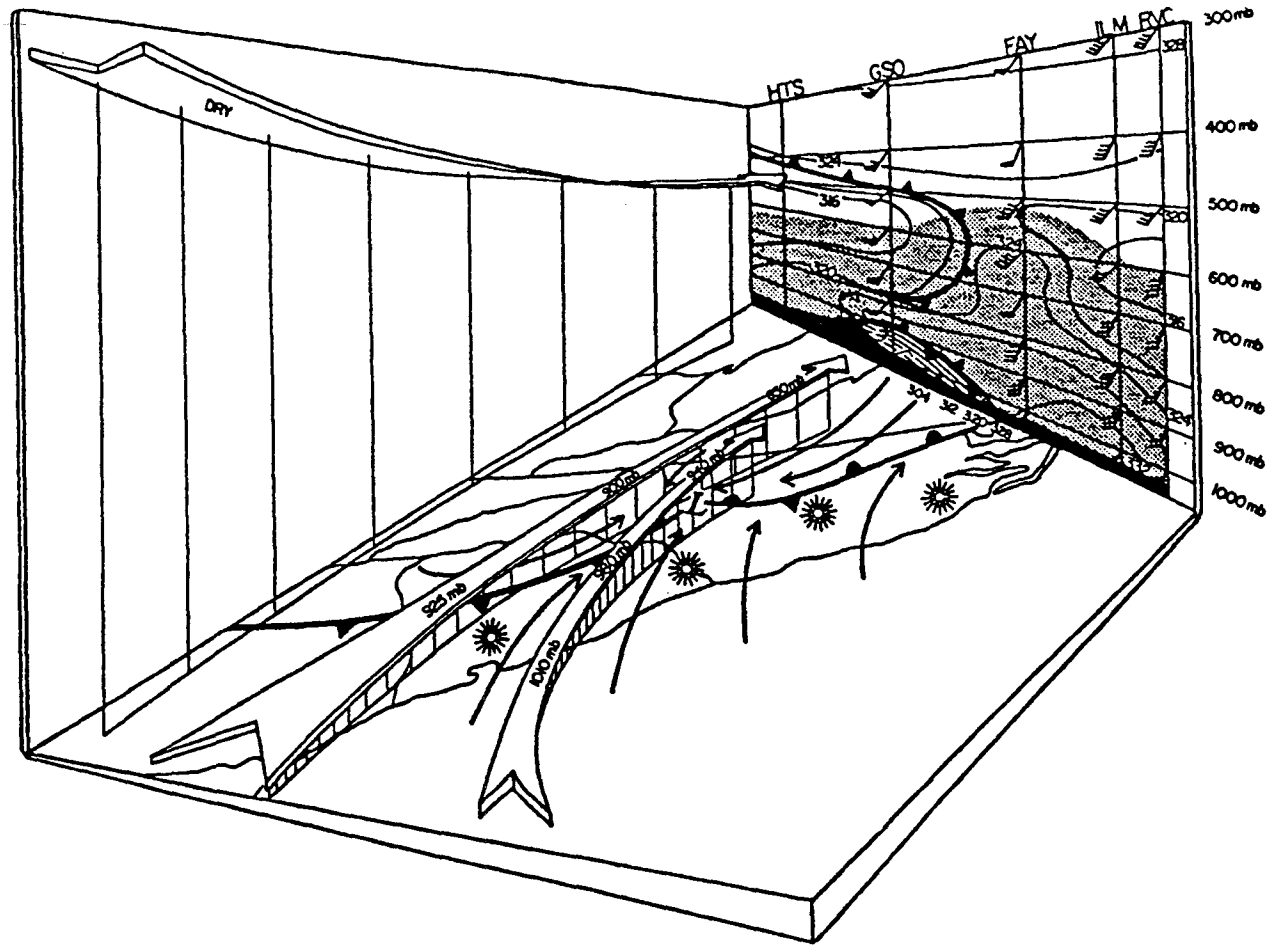


FIG. 10. Conceptual model at the time of the severe weather outbreak (1800 UTC 13 March 1986) as depicted by Businger et al. (1990). Surface coastal front depicted, solid arrows indicate surface streamlines, open arrows indicate airflow trajectories aloft. Sun symbols indicate area of strongest diabatic heating due to solar insolation. Back walls (1800 UTC) cross section from RVC to GSO: contours are equivalent potential temperature (in Kelvin), rawindsonde winds are shown with the usual convention (flag = 25 m $s^{-1}$, barb = 5 m $s^{-1}$, half-barb = 2.5 m $s^{-1}$), shading indicates area with decreasing equivalent potential temperature with height.

turbance magnitudes this class of flows develop more slowly than the first class. Nevertheless, the continuous conversion of latent energy to perturbation energy in ascent regions suggests that this process, albeit slow in comparison to the first class, is robust and independent of perturbation amplitude and magnitude of $R_0$ provided $0 < R_0 < 1$. Recall the dramatic enhancement of surface frontogenesis resulting from the addition of nonuniform interior potential vorticity in examples of the first class. If one were to add to the second class of disturbances a positive interior potential vorticity anomaly displaced upstream of the positive $\theta$ perturbation along $Z = 0$, previous results imply a dramatic increase in the rate of surface development. Observations of moist surface development and its association with upper-level forcing are needed to further clarify these ideas.

A widely accepted representation of latent heat release in mid-latitude surface fronts and cyclones is obtained by reducing $N_0^2$. The absence of water in downdrafts suggests that a more accurate parameterization of latent heat release is to reduce $N_0^2$ in ascent regions only. However even this improvement is not sufficient. The dynamics given by (2.4) show that moist processes enter the balance equations (2.4d), (2.4e) asymmetrically by only changing the effective static stability for the cross-frontal equation (2.4e) while leaving equation (2.4d), relating $Q_g$ to $\Phi$, unchanged. Thus, the effect of latent heat release is more subtle than simply reducing $N_0^2$ in both balance equations in updraft regions. For short wavelength disturbances with initially uniform potential vorticity we have shown that, despite the deep extent of ascending motion in neutrally stable regions, there is little baroclinic coupling between the disturbance aloft and the induced surface potential vorticity. Clearly, if we were to reduce the overall static stability in ascent regions in both balance equations and run the dry model with the same disturbances, we

TABLE 2. Summary of three simulation experiments A, B, and C with the initial condition (3.2) at different amplitudes. Shown are nondimensional surface maxima at increasing times for the Jacobian, meridional velocity, and anomalous dry potential vorticity listed as $J$, $v_g$, and $q_g$, respectively. One nondimensional time unit corresponds to 9.25 h.

| Experiment A: Maximum $v_g$ = 7.3 m s$^{-1}$ | | | | |
|---|---|---|---|---|
| | $T$ = 0.0 | $T$ = 2.0 | $T$ = 4.0 | $T$ = 6.8 |
| $J$ | 1.41 | 1.58 | 2.76 | 21.11 |
| $v_g$ | 0.073 | 0.097 | 0.126 | 0.189 |
| $q_g$ | 0.00 | 1.17 | 2.97 | 4.72 |
| **Experiment B: Maximum $v_g$ = 3.65 m s$^{-1}$** | | | | |
| | $T$ = 0.0 | $T$ = 4.0 | $T$ = 8.0 | $T$ = 11.44 |
| $J$ | 1.17 | 1.44 | 2.64 | 20.14 |
| $v_g$ | 0.036 | 0.059 | 0.135 | 0.27 |
| $q_g$ | 0.00 | 0.782 | 5.37 | 78.53 |
| **Experiment C: Maximum $v_g$ = 14.7 m s$^{-1}$** | | | | |
| | $T$ = 0.0 | $T$ = 1.0 | $T$ = 2.0 | $T$ = 2.64 |
| $J$ | 2.42 | 1.99 | 4.99 | 50.32 |
| $v_g$ | 0.147 | 0.161 | 0.204 | 0.236 |
| $q_g$ | 0.00 | 1.51 | 6.96 | 50.32 |

would find substantial baroclinic coupling and in some cases rapid surface frontogenesis. In other words, the naive procedure accentuates baroclinic coupling for short wavelength disturbances—especially those with uniform potential vorticity.

Recently Businger, Bauman, and Watson (1990) investigated the evolution of a coastal front and an associated outbreak of severe weather over North Carolina. A unique feature of this study is the implication of a midtropospheric cold front or equivalently an interior potential vorticity maximum of short zonal scale in the initiation of a squall line along a coastal surface front. In terms of ideas developed here the squall line results from the interaction between the coastal surface front and the eastwardly propagating upper vorticity maximum. Figure 10, taken from Businger et al. (1990), is a conceptual snapshot of the passage of an advancing upper cold front of southerly dry air over the coastal front system. The near two-dimensionality of the flow is evident. Also, we note a deep moist region with relative humidities ranging from 70%–90% indicated by shading in the path of the upper cold front. The equivalent potential temperature $\theta_e$ is contoured with solid lines on the back wall and the decrease of $\theta_e$ with height underneath the upper vorticity maximum indicates vertical instability. Strictly speaking, in terms of the semigeostrophic model, the vertically unstable air corresponds to a negative $R$ parameter. Nevertheless let us accept as a first approximation, the assumptions made in section 2, taking $R$ very small, positive, and uniform. The third and fourth examples of section 3a provide simple descriptions for the genesis of this squall line system. Specifically, the rapid induction of surface potential vorticity; the interaction between the surface vorticity and the disturbance aloft; the eastward propagation of the vorticity couplet system and the narrow region of ascending motion above the surface vorticity maximum are characteristics similar to the process described in this observational study. The same upper vorticity maximum is implicated in the initiation of a squall line system at an earlier time over the lower Mississippi valley which dissipates before reaching the coastal front system. In broader scope we advance the hypothesis that the model results of section 3a provide a simple phenomenological description of squall-line genesis and the importance of:

1) a strong surface "seed" field,
2) small moist stability,
3) interior potential vorticity aloft,

in producing a surface system that intensifies and collapses to frontal scale. More observations similar to Businger et al. (1990) are called for to further understand the role of upper potential vorticity disturbances in the genesis of squall line systems.

Induced self-development often involves a three stage process consisting of potential vorticity induction at the surface forced by an upper-level disturbance, baroclinic interaction between potential vorticity structures, and finally a slow intensification of surface winds through the nonbaroclinic growth mechanism previously discussed. A recent diagnostic study of polar lows by Nordeng (1990) views the development as a two-stage process consisting of a transient baroclinic interaction between an upper-level trough and surface disturbance in accord with the ideas of Farrell (1984) followed by an air–sea interaction instability of the type discussed by Emanuel (1986) and Rotunno and Emanuel (1987) for tropical cyclones. However, the above examples model polar low development as an initial baroclinic growth phase followed by a prolonged slow intensification due to diabatic effects. Obviously, the highly three-dimensional flow associated with intensifying polar lows discussed by Nordeng (1990) cannot be completely captured by a two-dimensional model. In particular the two-dimensional flow excludes gradient wind balance which for deep cyclones or polar lows may substantially add to the pressure drop.

The model used in this paper has limitations of which perhaps the most important are:

1) the neglect of wave–mean flow interactions,
2) the neglect of three-dimensional processes,
3) the neglect of friction along the horizontal surfaces.

The two-dimensional Eady model precludes most interactions of the disturbances with the mean flow. For a more realistic three-dimensional problem there will be large changes in the basic state as the disturbances extract available potential energy from it. This interaction would modify the instantaneous growth rate

of the disturbances and could significantly alter the resulting frontal structures formed. For instance with a meridionally limited basic state, growing disturbances tend to decrease $\partial\bar{\theta}/\partial Y$ due to divergence of the wave induced heat flux. This is particularly true with the second class since their intensification is strongly dependent upon the meridional temperature gradient.

Another limitation of the model concerns the lower surface boundary condition. Significant progress has been made (Blumen and Wu 1983) for the semigeostrophic approximation in formulating a self-consistent boundary condition which would be applied at the top of an Ekman layer. As discussed in previous work (Farrell 1985; Montgomery and Farrell 1990), typical values of the effective boundary layer eddy viscosity of 5 $m^2$ $s^{-1}$ reduces the growth rate of exponentially growing modes of the dry Eady model, although transient development associated with interior potential vorticity disturbances is rapid, robust, and fairly insensitive to the presence of Ekman damping. Similar conclusions hold for short wavelength potential vorticity disturbances. Applying this reasoning to the damped moist frontogenesis model suggest that transient processes associated with interior potential vorticity may remain the predominant frontogenetic agents. Finally, for small to moderate Ekman numbers, equilibration for both of the above flow classes is possible.

The two-dimensional semigeostrophic Eady model is the accepted paradigm for surface frontogenesis in association with intensifying baroclinic waves. Despite its limitations this model provides a simple phenomenological description of the role of interior potential vorticity in surface frontogenesis. The initial value problem permits study of a general class of disturbances and focuses on the physical objects of the theory, namely the potential vorticity structures, rather than the mathematical objects which are the normal modes. The results reported exhibit a rich variety of processes associated with nonuniform potential vorticity disturbances. Further observations of tropospheric potential vorticity anomalies are indicated to determine realistic potential vorticity structures; the dynamics of which are central to the formation of atmospheric fronts.

*Acknowledgments.* This work was supported by NSF ATM-8712995 and NSF ATM-8912432. Dr. Donald Anderson graciously lent advice on numerical methods. Dr. Allan Robinson generously provided plotting resources. We would like to thank Dr. Kerry Emanuel and Dr. Chris Davis for their helpful comments on this work. Finally, we appreciate the constructive comments of the reviewers.

## REFERENCES

Blumen, W., 1980: A comparison between the Hoskins–Bretherton Model of frontogenesis and the analysis of an intense surface frontal zone. *J. Atmos. Sci.*, **37**, 64–77.

——, and R. Wu, 1982: An analysis of Ekman boundary layer dynamics incorporating the geostrophic momentum approximation. *J. Atmos. Sci.*, **39**, 1774–1782.

——, and ——, 1983: Baroclinic instability and frontogenesis with Ekman boundary layer dynamics incorporating the geostrophic momentum approximation. *J. Atmos. Sci.*, **40**, 2630–2637.

Bretherton, F. P., 1966: Critical layer instability in baroclinic flows. *Quart. J. Roy. Meteor. Sci.*, **92**, 325–334.

Businger, S., W. H. Bauman and G. H. Watson, 1990: Coastal frontogenesis and associated outbreak of severe weather on 13 March 1986. *Mon. Wea. Rev.*, submitted.

Charney, J., and A. Eliassen, 1964: On the growth of the hurricane depression. *J. Atmos. Sci.*, **21**, 68–75.

Davis, C., 1990: Cyclogenesis diagnosed with potential vorticity. Ph.D. thesis, Massachusetts Institute of Technology.

Eliassen, A., and E. Kleinschmidt, 1957: Dynamic meteorology. *Handbuch der Physik*, Springer Verlag, 1–154.

Emanuel, K. A., 1986: An air–sea interaction theory for tropical cyclones. Part I: Steady-state maintenance. *J. Atmos. Sci.*, **43**, 585–604.

——, M. Fantini and A. J. Thorpe, 1987: Baroclinic instability in an environment of small stability to slantwise moist convection. Part I: Two-dimensional models. *J. Atmos. Sci.*, **44**, 1559–1573.

Farrell, B. F., 1982: The initial growth of disturbances in a baroclinic flow. *J. Atmos. Sci.*, **39**, 1663–1686.

——, 1984: Modal and nonmodal baroclinic waves. *J. Atmos. Sci.*, **41**, 668–673.

——, 1985: Transient growth of damped baroclinic waves. *J. Atmos. Sci.*, **42**, 2178–2727.

Hoskins, B. J., 1975: The geostrophic momentum approximation and the semigeostrophic equations. *J. Atmos. Sci.*, **32**, 233–242.

——, and F. P. Bretherton, 1972: Atmospheric frontogenesis models: mathemtical formulation and solution. *J. Atmos. Sci.*, **29**, 11–37.

——, M. E. McIntyre and A. W. Robertson, 1985: On the use and significance of potential vorticity maps. *Quart. J. Roy. Meteor. Soc.*, **111**, 877–946.

Joly, A., and A. J. Thorpe, 1989: Warm and occluded fronts in two-dimensional moist baroclinic instability. *Quart. J. Roy. Meteor. Soc.*, **115**, 513–534.

Kleinschmidt, E., 1950: Uber den Auflbau und Entstehung von Zyklonen II. *Meteorol. Rundsch.*, **2**, 54–61.

Mak, M., 1982: On moist quasi-geostrophic baroclinic instability. *J. Atmos. Sci.*, **39**, 2028–2037.

Montgomery, M. T., and B. F. Farrell, 1990: Dry surface frontogenesis arising from interior potential vorticity perturbations in a semigeostrophic model. *J. Atmos. Sci.*, **47**, 2837–2852.

Nordeng, T. E., 1990: A model-based diagnostic study of the development and maintenance mechanism of two polar lows. *Tellus*, **42A**, 92–108.

Press, W. H., B. P. Flannery, S. A. Teukolsky and W. T. Vetterling, 1986: *Numerical Recipes, The Art of Scientific Computing*, Cambridge University Press, 818 pp.

Rotunno, R., and K. A. Emanuel, 1987: An air–sea interaction theory for tropical cyclones. Part II: Evolutionary study using a nonhydrostatic axisymmetric numerical model. *J. Atmos. Sci.*, **44**, 561.

Snyder, C., and R. S. Lindzen, 1990: Quasi-geostrophic wave-CISK in an unbounded baroclinic shear. *J. Atmos. Sci.*, **48**, 76–86.

Stevens, D. E., and R. S. Lindzen, 1978: Tropical wave-CISK with a moisture budget and cumulus friction. *J. Atmos. Sci.*, **35**, 940–961.

Thorpe, A. J., and K. A. Emanuel, 1985: Frontogenesis in the presence of small stability to slantwise convection. *J. Atmos. Sci.*, **42**, 1809–1824.

Whitaker, J. S., L. W. Uccellini and K. F. Brill, 1988: A model-based diagnostic study of the rapid development phase of the Presidents' Day cyclone. *Mon. Wea. Rev.*, **116**, 2337–2365.

Williams, R. T., 1967: Atmospheric frontogenesis: A numerical experiment. *J. Atmos. Sci.*, **24**, 627–641.